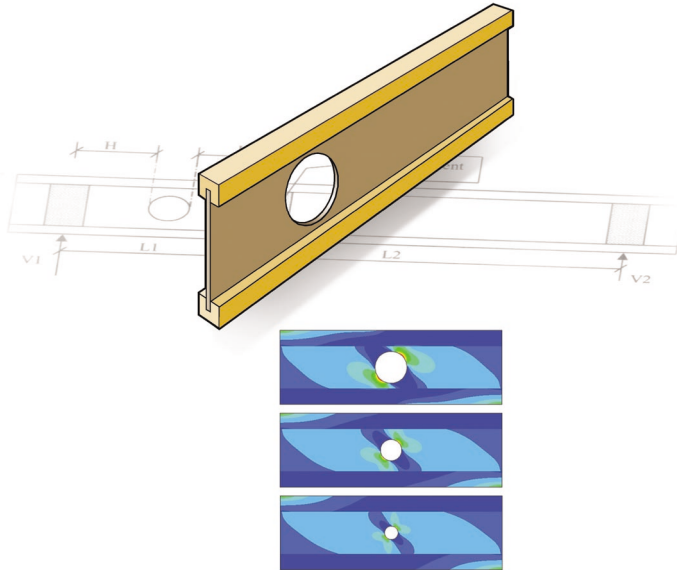




LUND
UNIVERSITY



STRENGTH ANALYSES OF WOODEN I-BEAMS WITH A HOLE IN THE WEB

REGINA HERMELIN

Structural
Mechanics

Master's Dissertation

Structural Mechanics

ISRN LUTVDG/TVSM--06/5138--SE (1-74)

ISSN 0281-6679

STRENGTH ANALYSES
OF WOODEN I-BEAMS
WITH A HOLE IN THE WEB

Master's Dissertation by
Regina Hermelin

Supervisors:

Per Johan Gustafsson and Erik Serrano,
Div. of Structural Mechanics

Copyright © 2006 by Structural Mechanics, LTH, Sweden.
Printed by KFS I Lund AB, Lund, Sweden, February, 2006.

For information, address:

Division of Structural Mechanics, LTH, Lund University, Box 118, SE-221 00 Lund, Sweden.
Homepage: <http://www.byggmek.lth.se>

Acknowledgements

The work presented in this master's thesis was carried out during the autumn and winter 2005/2006 at the Division of Structural Mechanics at Lund Institute of Technology in Sweden.

I would like to thank my supervisors Prof. Per Johan Gustafsson and Dr. Erik Serrano, for sacrificing their time, for valuable discussions and for their guidance throughout the work with this thesis.

Lund, January 2006

Regina Hermelin

Abstract

Wood-based light-weight I-beams are today widely used in the construction industry. An important feature of these beams is that the user can make holes in the web where needed. Today there is no general method used to calculate the reduced strength of these beams with a hole in the web. The calculation methods vary between the manufacturers and are commonly based on empirical results. The aim of this master's thesis was to create finite element models of this type of beams and with these investigate the stress distribution in beams with holes in the web, where a crack would likely occur and in what direction it will grow. The aim was furthermore to calculate the shear force capacity for beams with holes by use of different models based on fracture mechanics theory, as well as investigate how changes in the material properties influence the shear force capacity, and finally to evaluate the currently used calculation methods and suggest improvements or a new method.

Calculations showing the location of the most stressed point and the orientation of the principal stresses in an area surrounding this point were performed for a number of load cases. For load cases dominated by shear force the results indicated diagonal cracking in 45° direction. The load cases with pure normal or moment loading indicated fracture in the upper or lower edge of the hole. Furthermore, the calculated stresses indicated that a crack would both initiate and continue to grow along an approximately straight line perpendicular to the edge of the hole.

Three methods based on fracture mechanics were used in the finite element calculations of the shear force capacity; the point stress criterion, the mean stress criterion and the initial crack criterion. The calculated shear force capacity from these methods was compared to the shear force capacity gained in a previously performed test study. In this study 11 beam geometries were tested, and to be able to compare the calculations, the same geometries and load cases were used in the present study. The results show that the mean stress criterion and the initial crack criterion are suitable for shear force capacity calculations for beams with holes in the web. The point stress criterion severely underestimated the shear force capacity for some beams. The calculation method used by the manufacturers Swelite and Forestia was evaluated by comparing the results from the test study with the results from using this method. This comparison showed that this method overestimated the real shear force capacity for one beam. A new calculation method can be based on the mean stress criterion, since this method gave values well corresponding to the results from the test study and since this is a fairly easy method to use.

Sammanfattning

Träbaserade lättbalkar är idag vanligt förekommande i byggnadsindustrin. En viktig egenskap hos dessa balkar är att användaren kan göra hål i livet där det behövs, för installationer eller liknande. Idag finns det dock ingen allmänt använd metod för att beräkna den reducerade tvärkraftskapaciteten för dessa balkar med hål i livet. Beräkningsmetoderna varierar mellan de olika tillverkarna och är vanligtvis baserade på empiriska resultat. Syftet med detta examensarbete var att skapa finita elementmodeller av denna typ av balk och med dessa undersöka spänningsfördelningen i balkar med hål i livet, samt var en spricka troligtvis uppkommer och i vilken riktning den sedan växer. Syftet var vidare att beräkna tvärkraftskapaciteten för balkar med hål med hjälp av olika modeller baserade på brottmekanik, samt att undersöka hur förändringar av de ingående materialens egenskaper påverkar tvärkraftskapaciteten, och slutligen utvärdera nuvarande beräkningsmetoder samt föreslå förbättringar eller en ny metod.

Beräkningar som visade läget för den mest ansträngda punkten och huvudspänningarnas orientering i ett område runt denna punkt gjordes för ett antal olika lastfall. För lastfall dominerade av tvärkraft indikerade resultaten diagonal sprickbildning i 45°-riktning. Belastning med enbart normalkraft eller moment indikerade brott i hålets övre eller undre kant. Beräknade spänningar indikerade vidare att en brottspricka både initieras och sedan fortsätter att propagera ungefär längs en rak linje vinkelrätt mot hålets kant.

Tre metoder baserade på brottmekanik användes i finita elementberäkningarna av tvärkraftskapaciteten; punktspänningskriteriet, medelspänningskriteriet och initialsprickakriteriet. Den beräknade tvärkraftskapaciteten från dessa metoder jämfördes med tvärkraftskapaciteten från tidigare provningar av 11 olika balkgeometrier, och för att göra beräkningarna jämförbara användes samma geometrier och lastfall i denna studie. Resultaten visade att medelspänningskriteriet och initialsprickakriteriet är lämpliga för beräkning av den reducerade tvärkraftskapaciteten hos balkar med hål i livet. Punktspänningskriteriet underskattade tvärkraftskapaciteten kraftigt för några balkar. Beräkningsmetoden som används av de två nordiska tillverkarna Swelite och Forestia utvärderades genom jämförelse mellan resultat från provningarna och resultat från denna metod. Denna jämförelse visade att beräkningsmetoden över-skattade den verkliga tvärkraftskapaciteten för en balk. En ny beräkningsmetod föreslås baseras på medelspänningskriteriet, då denna metod gav värden som väl överrensstämde med resultaten från provningarna, samt då denna metod är tämligen enkel att använda.

Contents

1	Introduction	1
1.1	Background	1
1.2	Objectives	2
1.3	Limitations	2
1.4	Audience	3
1.5	Methodology	3
1.6	Disposition	3
2	Theory	5
2.1	Wood-based light-weight I-beams	5
2.2	Current calculation methods	6
2.2.1	FinnForest	6
2.2.2	Swelite	7
2.2.3	Forestia	8
2.3	Beam failure	8
2.4	Fracture Mechanics	9
2.4.1	The point stress criterion	10
2.4.2	The mean stress criterion	10
2.4.3	The initial crack criterion	12
2.5	Materials	14
3	Stress distribution and crack location and orientation	17
3.1	The model	17
3.2	Pure normal, shear and moment loading	19
3.2.1	Method	19
3.2.2	Results	20
3.2.3	Discussion	23
3.3	Combined load cases	23
3.3.1	Method	23
3.3.2	Results	24
3.4	Conclusions	27

4	Beam strength calculations by means of three fracture criteria	29
4.1	Beam geometries	29
4.2	Converting point load to shear force	30
4.3	Summary of results from beam tests	31
4.4	Finite Element calculations	31
4.5	Location and growth direction for cracks	32
4.6	The point stress criterion	33
4.6.1	Method	33
4.6.2	Results	33
4.7	The mean stress criterion	34
4.7.1	Method	34
4.7.2	Results	35
4.7.3	Discussion	36
4.8	The initial crack criterion	37
4.8.1	Method	37
4.8.2	Results	38
4.8.3	Discussion	40
4.9	Cracks that do not fit into the web	41
5	Evaluation and new calculation method	43
5.1	Evaluation of the calculation criteria	43
5.2	Evaluation of current calculation method	46
5.2.1	Method	46
5.2.2	Results	46
5.2.3	Discussion	47
5.3	Beam parameter study	48
5.3.1	Method	48
5.3.2	Results	49
5.4	New approximate strength equation	51
6	Conclusions	55
6.1	Concluding remarks	55
6.2	Future work	56
A	Stress distribution in beams	59
B	Mean stress plots	67

Chapter 1

Introduction

1.1 Background

Wood-based light-weight I-beams, also known as I-joists, are today widely used and accepted in the construction industry around the world. The beams are mainly used in floors, roofs and walls in residual buildings, and also to some extent in commercial constructions [8]. There are a number of manufacturers of wood-based light-weight I-beams on the Nordic market, for example the Swedish manufacturer Swelite, the Norwegian Forestia and the Finnish FinnForest.

The wood-based light-weight I-beams have many advantages. The beams have high stiffness and strength, low weight and are useful for long spans. Furthermore, compared with other building materials, they are environmentally beneficial. The wood material also allows for the user to easily cut the beam into proper dimensions and to cut holes in the web where needed [8] [1]. Figure 1.1 shows an I-beam with a hole in the web.

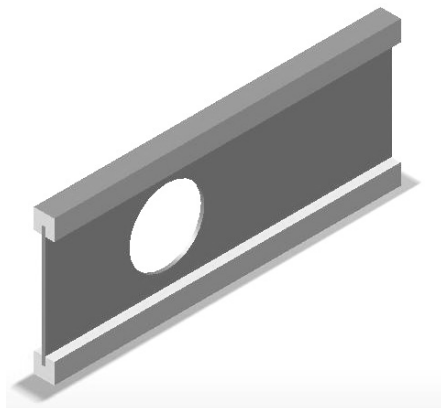


Figure 1.1: *Wood-based light-weight I-beam.*

When cutting a hole in the web, the manufacturers recommendations must be followed. The recommendations for making holes in webs differ between the manufacturers. Some manufacturers deliver the beams with pre-cut holes at certain locations, and do not allow for more holes over a certain diameter to be cut in the web [7]. Other manufacturers give equations or tables for calculating the reduced shear capacity after cutting holes in the web [15] [5]. There are no consistent methods used all over the construction industry for taking the impact of holes in the web into consideration. Today the user of the beams has to follow the guidelines of the particular manufacturer and these guidelines are commonly based on empirical data from beam tests.

1.2 Objectives

The objectives of this master's thesis are to:

- Create finite element models of wooden I-beams and investigate the stress distribution, the location for crack initiation as well as the crack growth direction for beams with holes in the web.
- Perform calculations with various fracture mechanics methods. These will be compared to results from beam tests in order to investigate how accurately they estimate the beams' strength.
- Investigate different material parameters' influence on the strength of the beams.
- Evaluate the methods recommended by the Nordic manufacturers for calculating the reduced shear capacity for I-beams with holes and suggest improvements or a new calculation method.

1.3 Limitations

In a previous report, Morris et al. [11] suggest that for a beam with a hole, failure will initiate where the stress at the edge of the hole exceeds the maximum stress capacity, and therefore, this report will be focused on failure in the web. The mode of fracture is furthermore assumed to be of type I, the opening mode, see Section 2.4. This corresponds to the assumption of isotropic properties of the web material. This material is assumed to be linear elastic. Possible influences of geometrical instabilities and large non-linear deformations are not considered in the present study. Neither is possible influences from climatic variations or long duration of loading considered.

1.4 Audience

To fully comprehend this thesis, some knowledge in structural mechanics, the finite element method and wood is required, but most important is a keen interest in wood-based building materials and their features.

1.5 Methodology

First the stress distribution and possible crack direction in beams with cut holes were investigated by modeling beams with different hole diameters and applied load cases in a finite element program. The program used was ABAQUS 6.5. The results from this investigation were used in the next step, where certain beams were modeled and analyzed with respect to strength. The beams analyzed had the same geometry and type of loading as the beams tested in a previous experimental study [14]. The calculations were performed for three different criteria, that were established by studying fracture mechanics theories. The results from the calculations were evaluated and the influences from the material parameters were studied. The final task was to evaluate the calculation methods recommended by the Nordic manufacturers and suggest improvements or other calculation methods that would better describe the true shear force capacity for wooden I-beams with cut holes. The plots in this thesis were made with MATLAB 7.0.4 and the report was written with L^AT_EX 2_ε.

1.6 Disposition

Chapter 2 includes the theory used in this study. The current calculation methods recommended by the Nordic manufacturers are brought to attention, as well as the fracture mechanics theories and the material properties that will be used in the calculations in the following chapters.

Chapter 3 is focused on the stress distribution and probable direction of crack growth in beams with holes. In this chapter finite element calculations are performed for beams with three hole diameters and for a range of load cases.

Chapter 4 deals with calculations of the shear force capacity for different beams with holes. These calculations were performed for three different criteria, that were described in Chapter 2.

In Chapter 5 the results from the use of the three criteria are evaluated. An additional parameter study is conducted, where the focus is on the material properties and the effect changes of these have on the shear force capacity. This chapter also includes an evaluation of the current calculation methods with respect to the results in Chapter 4 and suggestions for improving these calculation methods.

In Chapter 6 some conclusions are drawn and suggestions for future research are given.

Chapter 2

Theory

2.1 Wood-based light-weight I-beams

There are numerous manufacturers of wood-based light-weight I-beams, and they offer a range of web and flange materials and many different methods for calculating the shear capacity of beams with holes in the web. Georgia-Pacific produces an I-beam with a web made of Oriented Strand Board (OSB) with three pre-cut holes [7]. The Finnish manufacturer FinnForest produces an I-beam with a system of pre-made holes (knock-outs) in the web with a diameter of 38 mm and a distance between the holes of 300 mm. The web is made of OSB-board and the flanges of Laminated Veneer Lumber (LVL) [4]. The Swedish manufacturer Swelite produces a beam with a web made of 8 mm thick High Density Fibre Board (HDFB) and flanges made of solid wood [15]. The Norwegian manufacturer Forestia produces an I-beam with a web made of particle board and flanges made of solid wood [5]. Figure 2.1 shows one of the light-weight wood-based I-beams that Swelite offers to the market.

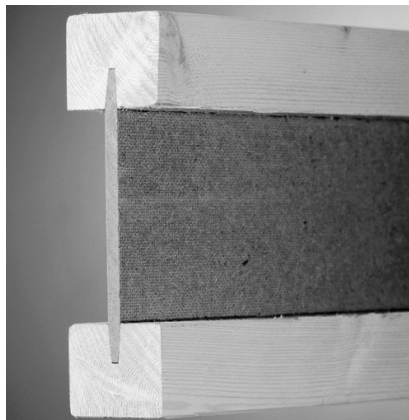


Figure 2.1: *One of Swelite's light-weight wood-based I-beams [9].*

2.2 Current calculation methods

This master's thesis will focus on the calculation methods suggested by the two Nordic manufacturers Swelite and Forestia. These two manufacturers do not provide pre-cut holes in the beams, but equations to take the reduced capacity of beams with cut holes into consideration. The Finnish manufacturer FinnForest's calculation method is not included, since this method is not comparable with those from Swelite and Forestia. However, FinnForest's calculation method will be brought to attention and its comparability will be discussed in the following section.

2.2.1 FinnForest

The Finnish manufacturer FinnForest produces an I-beam named Finnjoist I-joist that is provided with knock-out holes of diameter 38 mm and a 300 mm spacing between the centers of these holes. Additional holes can be cut in the web if certain restrictions are followed. The reduced characteristic shear force capacity $V_{k,hole}$ is then calculated with Equation 2.1 [4]. Figure 2.2 shows the cross-section of Finnjoist I-joist [4].

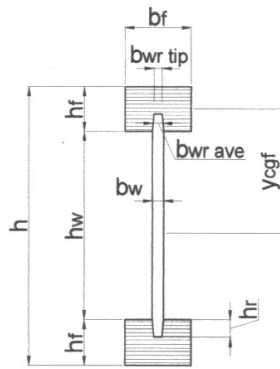


Figure 2.2: Cross-section of Finnjoist I-joist. Figure adopted from [4]

$$V_{k,hole} = 1.1k_{hole}V_k \leq V_k \quad (2.1)$$

where V_k is the characteristic shear capacity for the beam without the additional hole. The reduction factor k_{hole} is calculated with Equation 2.2 [4].

$$k_{hole} = \frac{h_w + h_f - k_{shape}h_{hole} - 38k}{h_{w,eff} - 38}, \quad 0 \leq k_{hole} \leq 1 \quad (2.2)$$

where h_w is the depth of the web and h_f is the flange depth. The factor k_{shape} is 1 for circular holes and 1.23 for rectangular holes and h_{hole} is the diameter in case of a circular hole and the largest side of the hole in case of a rectangular hole. The factor $h_{w,eff}$ is calculated with Equation 2.3 and the factor k with Equation 2.4 or Equation 2.5 [4]. The thickness of the web is denoted b_w and H is the total height of the beam.

$$h_{w,eff} = \frac{35b_w}{h_w}(h_w + h_f) \leq h_w + h_f \quad (2.3)$$

$$\text{For } H \leq 212 \text{ m: } k = \frac{250 - H - h_{hole}}{76}, \quad 0 \leq k \leq 1 \quad (2.4)$$

$$\text{For } H \geq 212 \text{ m: } k = \frac{H - h_{hole} - 174}{76}, \quad 0 \leq k \leq 1 \quad (2.5)$$

Holes with a diameter larger than 20 mm must be placed in the center of the web. The length between the edges of two holes should be no less than twice the diameter of the largest hole. If not, the two holes should be considered as one elongated hole [4]. However, since the distance between the knock-outs is $300 - 2 \cdot \frac{38}{2} = 262$ mm, the maximum allowed diameter of a hole placed between two knock-outs is 52.4 mm. Since only one beam from the tests used for comparison (see Section 4.1) had a hole diameter less than 52.4 mm, FinnForest's method for calculating the reduced shear force capacity is not suitable for comparison with the results from the calculation in the following chapters.

2.2.2 Swelite

The Swedish manufacturer Swelite uses an equation for calculating a reduction factor k , which reduces the shear capacity for beams with cut holes. Swelite also gives certain restrictions for how and where holes can be cut in the web. The distance between the edge of a hole and the support should be no less than the total depth, H , of the beam, see Figure 2.3. The same minimum distance should be used between the edges of two holes. Furthermore, the diameter, d , of the hole should be less than the depth of the web, h_w . All holes with a diameter d larger than 20 mm must be placed in the center of the depth of the web. Holes with smaller diameters can be placed at any position in the web, as long as the distance to the edge of another hole or to the support is at least 40 mm. The characteristic shear capacity $V_{k,hole}$, in the cross section at the center of the hole can be calculated with Equation 2.6 and Equation 2.7, based on the characteristic shear capacity of the beam without any hole, V_k .

$$V_{k,hole} = V_k \cdot k \quad (2.6)$$

$$k = \frac{H - h_f - 0.9d}{H - h_f} \quad (2.7)$$

where h_f is the depth of the flange.

Swelite's equations also apply for beams having rectangular holes, if the depth of the beam is less than 250 mm and the holes have corner radii of at least 20 mm. The width of a rectangular hole, w , should be less than the depth of the web, h_w , and the depth of the hole, h , should be less than half the depth of the web. If these requirements are fulfilled Equation 2.6 and Equation 2.7 still apply, with the difference that the diameter d is substituted with the largest of the sides of the hole [15].

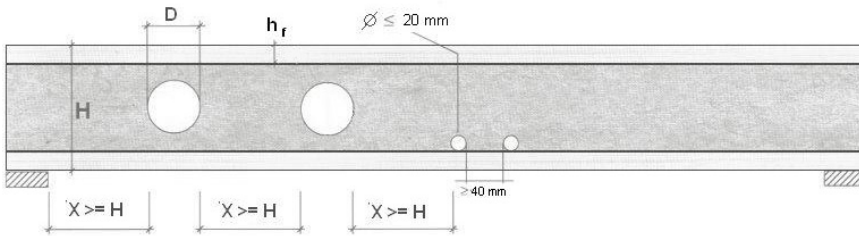


Figure 2.3: *Dimensions for Swelite's beams (figure was adopted from Swelite's recommendations) [15].*

2.2.3 Forestia

The Norwegian manufacturer Forestia uses the same equations as Swelite, Equation 2.6 and Equation 2.7, for their beams Rantibjelken, for calculating the characteristic shear capacity for beams with holes. Their restrictions are though somewhat different. Rectangular holes can have a maximum depth (h) equal to the depth of the web, h_w , under the condition that the width of the hole, w , is less than 150 mm. Furthermore, the characteristic shear capacity, V_k , in the section where the rectangular hole occurs should never exceed 4 kN [5].

2.3 Beam failure

Failure in the wood-based light-weight I-beams loaded in shear with transversal supports of the flanges can be caused not only by fracture in the web material, but also by buckling of the web and fracture along the web to flange adhesive joint [11]. Web buckling will only effect the capacity of HDFB beams when the ratio $h_w/b_w \geq 35$ [11] according to the Swedish code of practice and EC5, where h_w is the

depth of the web and b_w is the thickness of the web. With a web thickness of 8 mm, this results in a depth of the beam of at least 280 mm. Most beams used in this study have a depth of 220 mm, (see Chapter 3 and Chapter 4 for further information about used beams) and therefore, buckling will not be investigated further. Since Morris et al. in a previous report [11] suggest that failure in beams with holes will initiate in the web, fracture along the web to flange adhesive joint will neither be investigated.

Additionally, failure in the web needs to be defined precisely. Previous beam tests [14] showed that beams with holes will have cracks running from the edge of the hole to the web to flange joint on both the upper and lower side of the hole, after complete failure. This raises the question of how to define failure in the web. Should failure be considered as crack growth on one side or on both sides of the hole? If a crack starts to grow in the weakest point at the edge of the hole, the area over which to distribute the stresses on this side of the hole will be smaller. Thus, the stresses on the other side of the hole will increase and this can lead to crack initiation and growth on the other side of the hole. The increased magnitude of the stress on the other side of the hole results in a lower failure load needed for the second crack to initiate. Thus, the initiation of the first crack in the weakest point will decrease the failure load needed for initiation of the second crack on the other side of the hole, and therefore failure in the web will be defined as crack growth in the part with the weakest point throughout the rest of this master's thesis.

2.4 Fracture Mechanics

To calculate the shear force capacity of a beam with a hole in the web, different methods based on fracture mechanics can be used. Three methods will be used in this study and these will be described in this section. Two of them are based on linear elastic fracture mechanics theory (LEFM) and they are described by the following criteria: The point stress criterion, the mean stress criterion and the initial crack criterion [11]. The point stress criterion is conventional and widely used. The mean stress criterion and the initial crack criterion are more general methods and with these it is possible to study the influence from the material's strength, stiffness and fracture energy on the shear capacity of the beam [11]. The stress along a crack is small compared to the stress perpendicular to the crack, which is causing the crack to grow. Because of this the tensile strength of the web material, f_t , will be used throughout this study to determine the shear force capacity. The failure mode is thus assumed to be of type I; the opening mode, see Figure 2.4 [10]. For mode I, which is the most common failure mode in an isotropic material, the loads are applied normal to the crack plane.

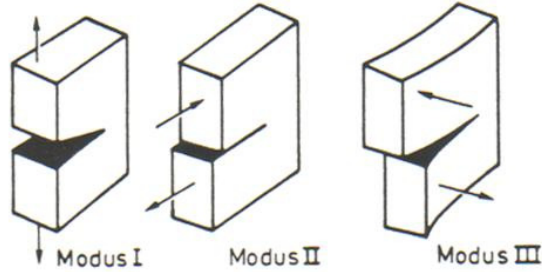


Figure 2.4: *The three types of failure mode [10].*

2.4.1 The point stress criterion

The point stress failure criterion is a well-known and conventional approach [11] and it is based on Equation 2.8.

$$\sigma_{1,max} = f_t \quad (2.8)$$

where f_t is the tensile strength of the material, $\sigma_{1,max}$ is the maximum of σ_1 in the vicinity of the hole and σ_1 is the first principal stress. When using this criterion to determine the shear force capacity of a beam, a crack is assumed to initiate in the most stressed point in the web and this crack initiation is furthermore assumed to give immediate failure of the beam. The load on the beam, P_f , causing a stress with the same magnitude as the tensile strength of the material, f_t , can easily be calculated if a load P is known to give the stress $\sigma_{1,max}$, see Equation 2.9.

$$P_f = \frac{f_t P}{\sigma_{1,max}} \quad (2.9)$$

For beams with holes in the web, the most stressed point in the web will be somewhere at the edge of the hole. The point stress criterion has the advantage that no actual crack needs to be modeled.

2.4.2 The mean stress criterion

With the mean stress failure criterion the mean stress of σ_1 (the first principal stress) over a certain length is used to calculate the failure load P_f , instead of the maximum

stress. According to this method, crack growth will occur when the mean stress, $\sigma_{1,mean}$, exceeds the tensile strength of the material, f_t . The assumed crack will initiate in one of the two points with local maximum stress, $\sigma_{1,max}$, at the edge of the hole. Since the mean stress over a distance will be less than the maximum stress over the same distance, the mean stress criterion will predict a failure load equal to or larger than the failure load predicted by the point stress criterion [6]. The length over which the mean stress is calculated is dependent on the web material. For brittle materials this length is small. For constructions without any sharp initial crack this failure criterion gives the same failure load as the point stress criterion, if the material is very brittle and/or the absolute measures of the construction are very large. For a construction made from a very brittle material with a sharp initial crack the criterion gives a failure load equal to that obtained using Linear Elastic Fracture Mechanics (LEFM). Using LEFM, the stress close to a sharp crack can be described by Equation 2.10 and Figure 2.5 [10].

$$\sigma_y = \frac{K_1}{\sqrt{2\pi x}} \quad (2.10)$$

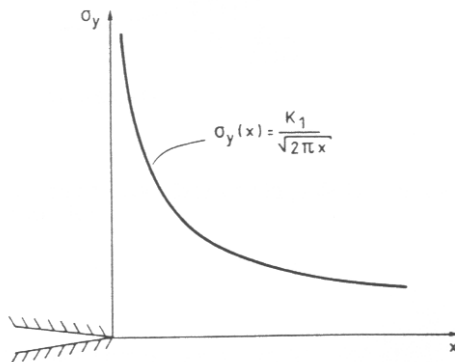


Figure 2.5: Stress distribution near a sharp crack, according to LEFM [10].

For an isotropic material subjected to plane stress the failure mode I stress intensity factor is $K_I^2 = EG$, where E is the Young's modulus and G is the mode I energy release rate. Integrating Equation 2.10 over a distance x gives the resulting force F .

$$F = b_w \int_0^x \sigma_y(x) dx = b_w \int_0^x \sqrt{\frac{EG}{2\pi x}} dx = 2b_w \sqrt{\frac{EG}{2\pi}} \sqrt{x} \quad (2.11)$$

where b_w is the thickness of the web. The mean stress over the distance x can be calculated with Equation 2.12.

$$\sigma_{1,mean} = \frac{F}{b_w x} = \sqrt{\frac{EG}{2\pi}} \frac{2}{\sqrt{x}} \quad (2.12)$$

A specific length x_0 is chosen so that the mean stress ($\sigma_{1,mean}$) over this length equals the tensile strength f_t of the material, and so that the energy release rate G equals the fracture energy G_f . This gives Equation 2.13 [10].

$$f_t = \sqrt{\frac{EG_f}{2\pi}} \frac{2}{\sqrt{x_0}} \Rightarrow x_0 = \frac{2 EG_f}{\pi f_t^2} \quad (2.13)$$

After the mean stress over this length has been calculated, the failure load acting on the beam can be calculated with Equation 2.14.

$$P_f = \frac{f_t P}{\sigma_{1,mean}} \quad (2.14)$$

where P is the external load which by means of some stress calculation method, e.g. the finite element method, is known to give the mean stress $\sigma_{1,mean}$. This method also has the advantage that no crack needs to be modeled.

2.4.3 The initial crack criterion

With the initial crack criterion a crack in the beam is introduced, starting from the point of the maximum of the first principal stress, $\sigma_{1,max}$, at the edge of the hole. The crack will have the initial length a_0 . The magnitude of a_0 is derived so that the failure load calculated from the initial crack criterion is the same as if calculated with LEFM for an infinite plate in a homogenous stress state. The stress intensity at the tip of the crack can be calculated with Equation 2.15 [6].

$$K_1 = \sigma \sqrt{\pi a_0} \quad (2.15)$$

Equation 2.15 is analogous with Equation 2.10 for the mean stress criterion. By replacing π in Equation 2.11 with $\frac{\pi}{2}$, and x with a_0 , the length a_0 can be derived in the same way as the derivation of x_0 . The magnitude of a_0 will then be half the magnitude of x_0 [6].

$$a_0 = \frac{x_0}{2} \quad (2.16)$$

When using the initial crack criterion in a finite element program, crack growth can be simulated by performing calculations for two cracks with different lengths. By simplification, the crack can be modeled according to Figure 2.6. This will result in a very sharp modeled crack that is not consistent with the geometry of a real crack tip. The real crack will be a distance x_a shorter than the modeled crack for four-node elements. Gustafsson [6] suggests that a reasonable assumption for the magnitude of the distance x_a is half the side length of the finite elements along the modeled crack. For the second calculation one node in the tip of the modeled crack will be opened and the crack will thus become one element side length longer. The real crack will grow the same length, but will still be x_a shorter than the modeled crack.

If x_a is equal to half the length of an element side, the length of the first modeled crack should be the same as a_0 . Then the mean value of the crack lengths for the two real cracks, a_1 and a_2 , will be the same as the length of the first modeled crack a_0 .

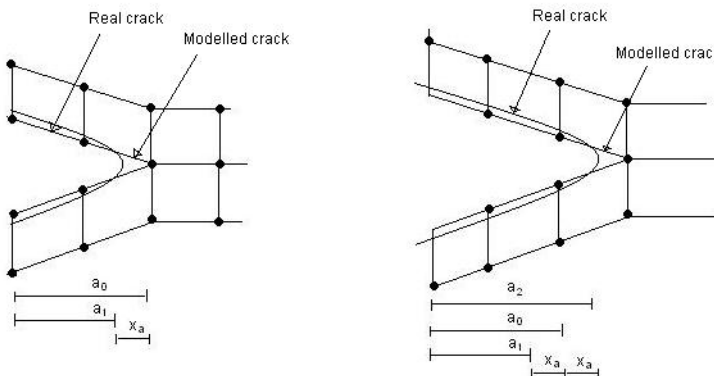


Figure 2.6: *Modeled crack in relation to the real crack.*

First the external work for the whole body, W , with the modeled crack of length a_0 is calculated, and then one node in the tip of the crack is opened to simulate crack

growth. The external work for the whole body is calculated with the new longer crack, $a_0 + 2x_a$. With the difference in external work for the two crack lengths and with the magnitude of these lengths, the energy release rate G can be calculated. The energy release rate G during crack extension, mode I, when the beam is loaded with a single load P can thus be expressed by Equation 2.17 [10].

$$G = \frac{P^2}{2b_w} \frac{\partial C}{\partial a} = \frac{\partial W}{b_w \partial a} \quad (2.17)$$

where C is the compliance and $\frac{\partial W}{\partial a}$ for $a = a_0$ is calculated with Equation 2.18.

$$\frac{\partial W}{\partial a} \simeq \frac{\Delta W}{\Delta a} = \frac{W_2 - W_1}{a_0 + 2x_a - a_0} = \frac{W_2 - W_1}{2x_a} \quad (2.18)$$

With the energy release rate G calculated for the load P , and the fracture energy G_f , the failure load P_f for the beam can be calculated with Equation 2.19.

$$\frac{P_f^2}{P^2} = \frac{G_f}{G} \quad \Rightarrow \quad P_f = P \sqrt{\frac{G_f}{G}} \quad (2.19)$$

2.5 Materials

The web material data used throughout this study is taken from a study by Morris et al. [11]. In this study the properties of the material used in beams manufactured by Masonite AB were examined. The web material was made from High Density Fibre Board (HDFB), in-plane isotropic, with a density $\rho = 950 \text{ kg/m}^3$. The thickness of the board, b_w , was 8 mm. From the material tests the average tensile strength $f_t = 30.0 \text{ MPa}$. Young's modulus for the web $E = 5748 \text{ MPa}$ and Poisson's ratio $\nu = 0.2$ [11].

The fracture energy, G_f , for the web material was also tested by Morris et al. A testing procedure for determining the fracture energy for tension perpendicular to the grain, (i. e. failure mode I, see Section 2.4) was used [12]. With this method a test specimen with a saw cut is tested during three-point bending by applying a load at midpoint and having the specimen simply supported in both ends [12]. The total work of fracture for two thicknesses, 40 mm and 80 mm, were calculated [11]. A small size effect was found, consistent with a previous study by Persson et al. [13]. Persson et al. suggest that an extrapolated value to zero sample size can be a relevant value for the real fracture energy [13]. The mean value of the total work

of fracture for the sample with thickness 40 mm was 3623 J/m² and for the 80 mm sample 3752 J/m². Thus, by extrapolation to 0 mm, the fracture energy $G_f = 3494$ J/m² [11].

The Young's modulus E for the flanges was set to 10 700 MPa in the direction along the fibres and to 550 MPa in the direction perpendicular to the fibres [2]. According to Burström [2] this is the properties for spruce. Poisson's ratio ν for the flanges where set to 0.25 [3]. In Table 2.1 all material properties used in the FE-calculations in this thesis are summarized.

Table 2.1: *The material parameters used in the FE-calculations.*

Web Material (HDFB)		Flange Material (spruce)	
f_t	30.0 MPa	$E_{//}$	10700 MPa
E	5748 MPa	E_{\perp}	550 MPa
ν	0.20	ν_{\perp}	0.25

Chapter 3

Stress distribution and crack location and orientation

This chapter deals with the distribution of stresses and the location and magnitude of the first of the maximum principal stress ($\sigma_{1,max}$) in I-beams with holes subjected to pure normal, shear and moment cross section forces. Stress images are presented to visualize how $\sigma_{1,max}$ is distributed in the beams for simple load cases. Some calculations will also be presented for load combinations to examine what influence different forces have on the total stress distribution in the beam. This will be used when making assumptions on where a crack will initiate and in what direction it will grow for different combined load cases.

3.1 The model

The geometrical model used to calculate the stress distribution had dimensions according to Figure 3.1 below. The thickness of the web, b_w , was set to 8 mm and the thickness of the flanges, b_f , to 47 mm. Swelite produces beams with this cross section and Forestia's Rantibjelken is also produced with the same cross section, except for the web thickness, which is 10 mm instead of 8 mm. The length of the beam was set so that the influence from the concentrated loads applied in the end of the beam would not affect the stress distribution in the area around the hole. According to Swelite's directives, the distance from the edge of a hole to a support should be no less than the depth of the beam, H [15]. Therefore, the total length of the beam models has been set to three times the depth of the beam. The calculations were performed for three different hole diameters d : 40.0, 63.0 and 94.5 mm. The holes were placed in the center of the beams during all calculations. The web and the flanges were modeled with material properties according to Section 2.5.

The beam was modeled with two-dimensional plane stress elements in ABAQUS. The web was made isotropic and the flanges were given the elastic type *lamina*, since they were made of solid wood and hence, were orthotropic. To achieve boundary conditions according to beam theory at the end of the beam and to enable simple

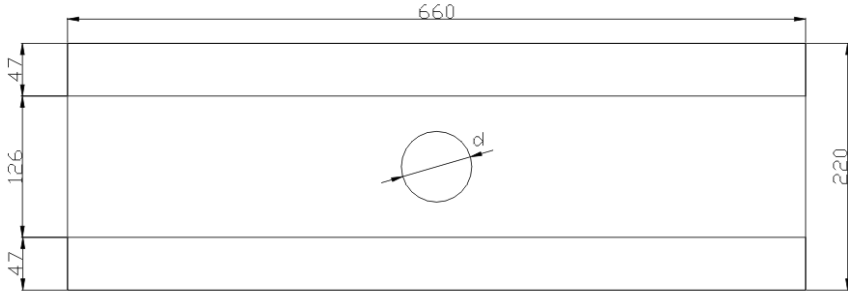


Figure 3.1: *Dimensions of the beam used to produce stress images.*

applications of normal, shear and bending moment loading, kinematic coupling constraints in ABAQUS were used to constrain the motion of the nodes in the beam ends to single points at the center of each end, respectively. These points, or nodes, each have three degrees of freedom; horizontal, vertical and rotation, corresponding to normal force, shear force and bending moment. The motion of the left end was constrained to zero in all directions. Loads were applied as concentrated forces and/or bending moments to the center point at the right end, in order to achieve the desired stresses in the beam.

In order to generate a suitable mesh, the beam was partitioned according to Figure 3.2. In the green areas in Figure 3.2, a structured meshing was used, and in the pink areas a free meshing technique with advancing front was used. Square, first order elements only were used for all beams and the element length in the area surrounding the hole (the pink area and the green inner circle) was set to approximately 1 mm. The remaining areas were meshed with an approximate element length of 3 mm. To visualize the meshes obtained, Figure 3.3 shows the mesh around the hole with 40 mm diameter.

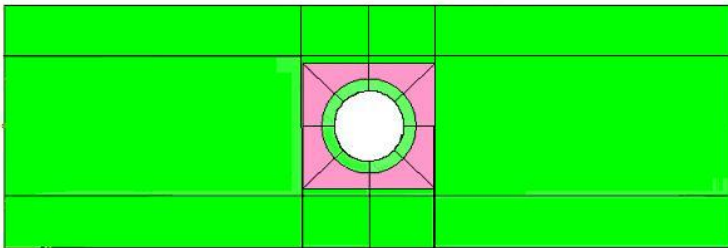


Figure 3.2: *Partitioning of the beam.*

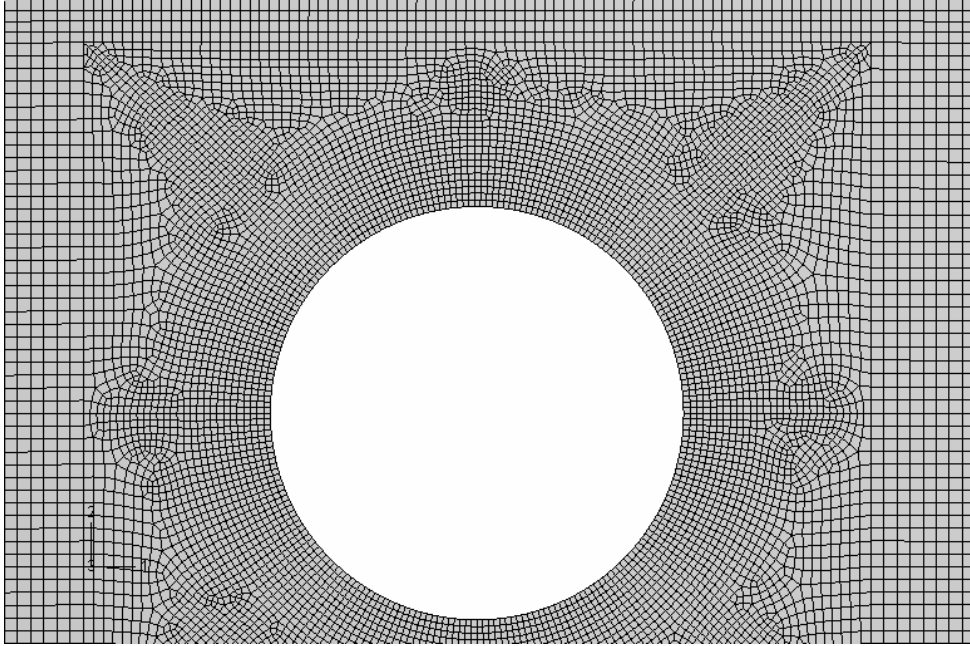


Figure 3.3: *The mesh around the hole.*

3.2 Pure normal, shear and moment loading

First, beams subjected to pure normal, shear and moment loads were studied.

3.2.1 Method

To estimate where a crack would likely occur, the first principal stress, σ_1 , along a path on the edge of the hole was calculated. For each element the stress was calculated in the corner points, i.e. the node points. The crack is most likely to initiate in the point with the maximum σ_1 ($\sigma_{1,max}$) at the edge. At the edge the orientation of the stress has the orientation of the edge. In order to estimate the direction of the growing crack in the beam, $\sigma_{1,max}$ was also calculated for two other paths. These paths form outer circles around the hole and are located approximately three mm and eight mm outside the edge of the hole, respectively. This was performed in order to investigate if $\sigma_{1,max}$ for these paths will occur at the same angles (see Figure 3.5) as $\sigma_{1,max}$ for the edge of the hole, and thus in a position perpendicular to the edge of the hole at the point with $\sigma_{1,max}$ at the hole edge. This would indicate that the crack will grow in a direction perpendicular to the edge of the hole, since it is likely that the crack growth will occur in the most stressed nodes. The Angle 1 and the Angle 2 (see Figure 3.5 and Table 3.1) that indicate the location of the maximum σ_1 are calculated from the maximum σ_1 that was found in the node-points, and are

thus indicating the location of the node with the maximum σ_1 .

All forces were applied at the right end of the beam. To achieve a pure normal force loading in the beam, a normal load of magnitude $1 \cdot 10^{-6}$ N was applied to the right end of the beam, pulling the beam horizontally. This was performed for the three different hole diameters. The influence of shear loading was also examined for the three hole diameters. To achieve pure shear force at the center of the hole, a shear force and a moment were applied at the right end of the beam. The shear force had a load of magnitude $1 \cdot 10^{-6}$ N. The moment was added to eliminate the moment effect caused by positioning the shear force at the end of the beam instead of at the center of the hole. This moment had a magnitude of $V \cdot L/2 = 1 \cdot 10^{-6} \cdot 660/2 = 330 \cdot 10^{-6}$ Nmm, where V is the shear force and L is the total length of the beam in mm. To achieve stress caused by pure moment load, a moment load of magnitude $1 \cdot 10^{-6}$ N in the negative direction was applied at the right end of the beam. Note however, that for the calculations of Angle 1 and Angle 2 (see Figure 3.5) the absolute magnitude of the forces is irrelevant for the results, while the ratios are of importance.

3.2.2 Results

The results from the calculations for beams subjected to pure normal and shear force and moment, respectively, are shown in Table 3.1. The notation (N, V, M) describes the cross section normal force, shear force and bending moment at the center of the hole, as in Figure 3.4. For the normal force and shear force loading, two maximum of the first principal stress σ_1 will occur, one on the upper side of the hole and one on the lower side. In Table 3.1, Angle 1 is the angle that indicates the location of $\sigma_{1,max}$ on the upper side of the hole and Angle 2 $\sigma_{1,max}$ on the lower side of the hole, as shown in Figure 3.5. The outer angles in Table 3.1 give the angles to the outer paths around the hole, approximately three and eight mm outside the edge of the hole, as mentioned earlier in Section 3.2.1. All angles are measured from the horizontal.

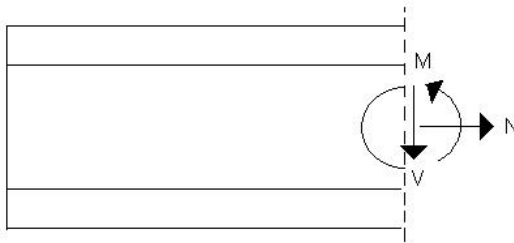


Figure 3.4: *Cross section forces and bending moment.*

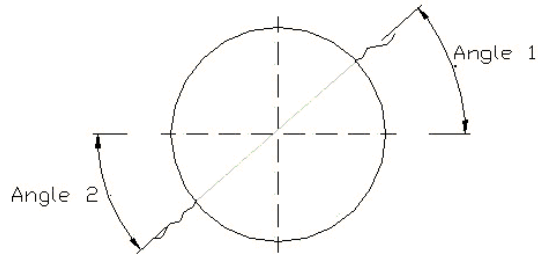


Figure 3.5: The maximum of the first principal stress $\sigma_{1,max}$ occurs at the edge of the hole in the direction indicated by Angle 1 and/or Angle 2.

Table 3.1: Location of maximum first principal stress, $\sigma_{1,max}$, of the pure load cases. N = Normal force, V = Shear force, M = bending Moment. The load combinations are described with the notation (N, V, M) , which relates to the forces acting in the centre of the hole.

Load case (N, V, M) [N, N, Nmm]	Hole diameter [mm]	Angle 1 [°]	1 st Outer Angle 1 [°]	2 nd Outer Angle 1 [°]	Angle 2 [°]	1 st Outer Angle 2 [°]	2 nd Outer Angle 2 [°]
(1 0 0) pure normal force	40.0	90.00	90.00	90.00	90.00	90.00	90.00
	63.0	89.34	84.40	90.52	90.00	90.00	90.00
	94.5	90.00	90.00	90.00	90.00	90.00	90.00
(0 -1 0) pure shear force	40.0	45.00	45.00	44.85	45.00	45.00	44.84
	63.0	44.86	44.86	44.85	44.84	44.84	44.84
	94.5	46.15	45.00	45.00	46.15	45.00	45.00
(0 0 -1) pure bending moment	40.0	-	-	-	90.00	90.00	90.00
	63.0	-	-	-	90.00	90.00	90.00
	94.5	-	-	-	90.00	90.00	90.00

The stress distributions in the beams subjected to the pure normal force are visualized in Figure 3.6. Figure 3.7 shows the stress distributions for the beams subjected to the pure shear force and Figure 3.8 shows the stress distributions for the beams subjected to stress from the bending moment.

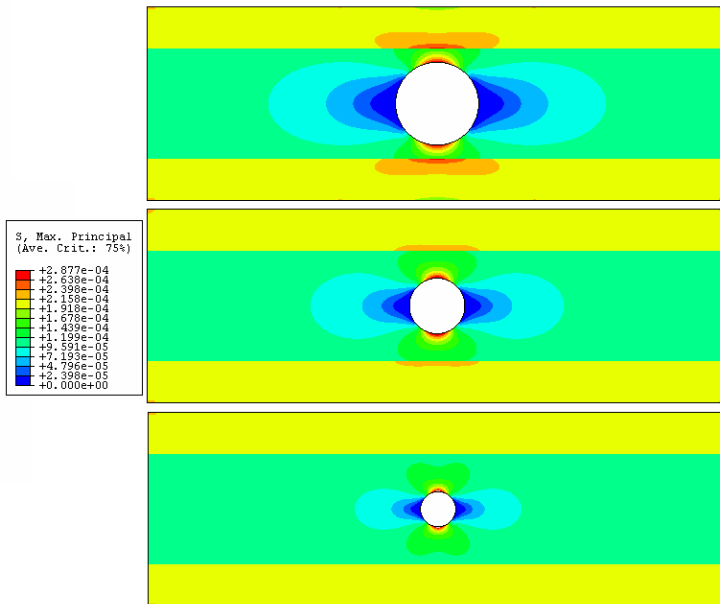


Figure 3.6: Distribution of σ_1 in beams subjected to pure normal force loading.

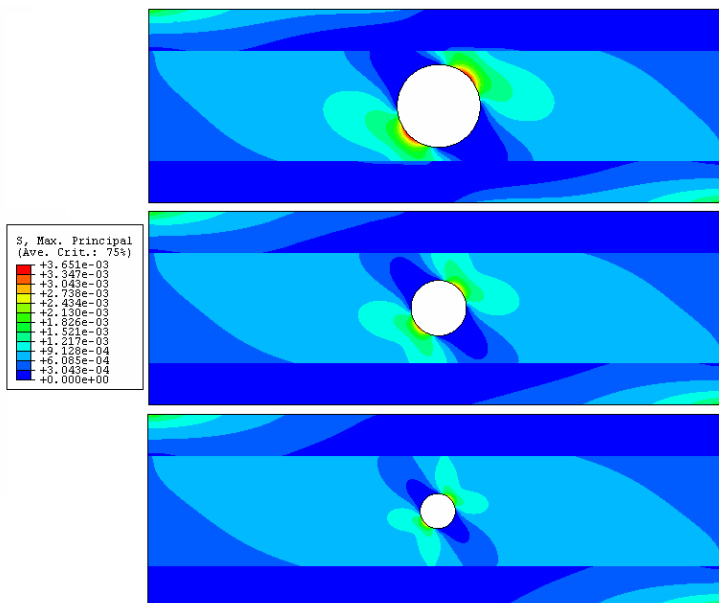


Figure 3.7: Distribution of σ_1 in beams subjected to pure shear force loading.

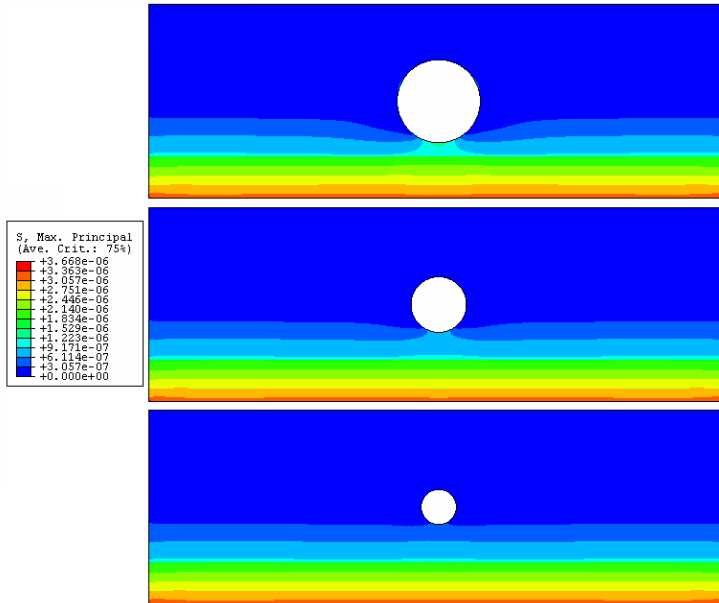


Figure 3.8: *Distribution of σ_1 in beams subjected to pure moment loading.*

3.2.3 Discussion

At pure shear force loading, the bending moment at the cross section of the hole is zero. But the bending moment has a small non-zero value at the section where the cracking will initiate, i. e. at the point where σ_1 has its maximum at the edge of the hole. The influence of this bending moment is however estimated to be small.

3.3 Combined load cases

In this section the locations of $\sigma_{1,max}$ and the direction of crack growth for combined load cases will be investigated.

3.3.1 Method

The same method as for the pure load cases was used, with the exception that all the load cases were calculated with the hole diameter of 63 mm. The used load cases are described by the notation (N, V, M) in Table 3.2, where N is the normal force, V is the shear force and M is the bending moment, in accordance with Figure 3.4.

To estimate the direction in which the crack will grow after initiation, besides investigation of the location of $\sigma_{1,max}$ for two outer paths, symbol plots were studied. In these plots the minimum principal stress, $\sigma_{1,min}$, was plotted in the area with the maximum principal stress $\sigma_{1,max}$ around the hole. If the arrows for $\sigma_{1,min}$ is

approximately in a straight line from the location of $\sigma_{1,max}$ at the hole edge to the location of $\sigma_{1,max}$ at the inner paths, the assumption that the crack will grow in this direction can be made. Crack growth will likely occur in the direction perpendicular to the maximum stress, hence, in the direction of the minimum stress.

3.3.2 Results

Table 3.2 shows the combined load cases that have been examined and the results obtained for the angles indicating the maximum of the first principal stress at circular paths around the hole. Stress distribution images for the different loading cases are available in Appendix A.

Table 3.2: Location of maximum first principal stress, $\sigma_{1,max}$, of the combined load cases.

Load case (N, V, M) N, N, Nmm]	Angle 1	1 st Outer Angle 1	2 nd Outer Angle 1	Angle 2	1 st Outer Angle 2	2 st Outer Angle 2
	[°]	[°]	[°]	[°]	[°]	[°]
$N/V = 0$						
(0 -1 -990)	52.75	52.74	54.30	40.19	40.19	37.10
(0 -1 -660)	49.60	49.59	51.15	41.73	41.73	40.19
(0 -3 -1320)	48.02	48.01	49.58	43.28	41.73	41.73
(0 -3 -770)	46.44	46.44	48.00	43.28	43.28	43.28
(0 -3 -660)	46.44	46.43	48.00	43.28	43.28	43.28
$N/V = -1$						
(1 -1 -990)	54.33	54.32	55.88	41.73	41.73	38.64
(1 -1 -660)	51.18	51.03	52.73	43.28	43.28	41.73
(3 -3 -1320)	49.60	40.59	51.15	44.84	44.84	43.28
(1 -1 -330)	49.60	40.59	49.58	44.84	44.84	44.84
(3 -3 -770)	48.02	48.01	49.58	44.84	44.84	44.84
(3 -3 -660)	48.02	48.01	49.58	44.84	44.84	44.84
$N/V = -1/3$						
(1 -3 -1320)	48.02	48.01	49.58	43.28	43.28	41.73
(1 -3 -770)	48.02	48.01	48.00	44.84	44.84	43.28
(1 -3 -660)	46.44	46.43	48.00	44.84	44.84	43.28
$N/V = -3$						
(3 -1 -990)	57.49	57.48	59.03	44.84	44.84	43.28
(3 -1 -660)	55.91	55.90	55.88	46.39	46.39	44.84
(3 -1 -330)	52.75	52.74	54.30	47.95	47.95	47.95

From the symbol plots it was clear that the directions of $\sigma_{1,min}$ make a straight line between the locations of $\sigma_{1,max}$ at the edge of the hole, and the locations of $\sigma_{1,max}$ at the two outer paths. This is also visual in Figure 3.9, which shows an example of a symbol plot visualizing $\sigma_{1,min}$.

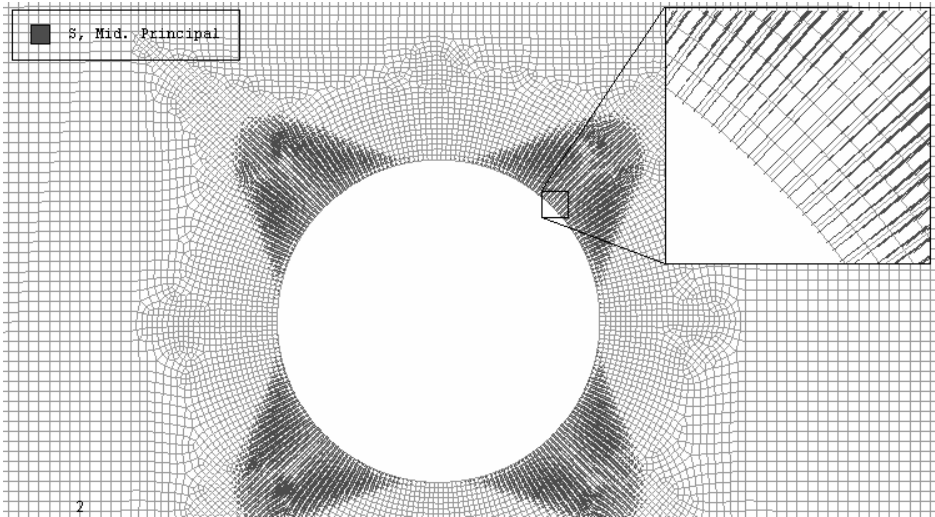


Figure 3.9: The directions of $\sigma_{1,min}$ around the hole.

For the calculations performed in later chapters, it is of interest to examine the influence normal and shear force and bending moment have on the angles to the locations of $\sigma_{1,max}$ around the hole in the combined load cases. This can be investigated by comparing the results from the load cases in Table 3.2. For this reason, two graphs have been made, see Figure 3.10 and 3.11. Figure 3.10 describes different load combinations' influence on Angle 1 and Angle 2 and Figure 3.11 shows the influence on the magnitude of $\sigma_{1,max}$. The right hand side of the diagrams in Figure 3.10 and 3.11 corresponds to shear force dominated loading. $V/(M/H)/(1 + V/(M/H)) = 1$ in the case of no bending moment, $M = 0$ and $V/(M/H)/(1 + V/(M/H)) = 0$ in the case of no shear force, $V = 0$. In Figure 3.10 and 3.11 H is the depth of the beams, which is 220 mm.

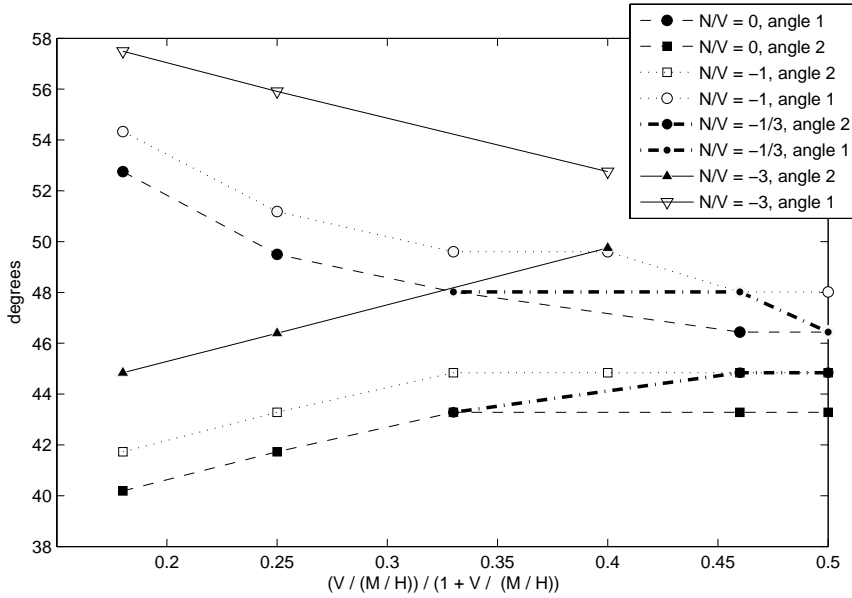


Figure 3.10: Angles to location of $\sigma_{1,max}$ at edge of hole.

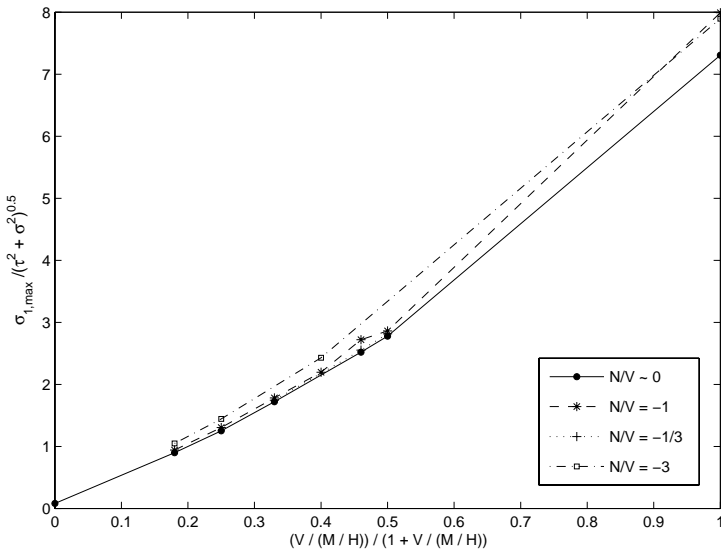


Figure 3.11: Magnitude of $(\sigma_{1,max})$ at edge of hole for different loads and beam geometries, normalized to $\sqrt{\tau^2 + \sigma^2}$, where $\tau = V/A_{web}$ and $\sigma = N/A + M/W$.

3.4 Conclusions

The conclusions that can be drawn from the calculations in this chapter are, first of all, that the location of the maximum of the first principal stress, $\sigma_{1,max}$, around the hole can differ significantly from 45° , depending on the load combination. In the calculations in the later chapters, it is therefore necessary to examine the location of $\sigma_{1,max}$ around the hole for each load case. Secondly, the angles to the locations of $\sigma_{1,max}$ at the two outer paths differ very little from the angle at the edge of the hole. The differences occur because the maximum σ_1 at the outer paths for some of the beams is located one or two nodes away along the path from the node that gives the same angle as for $\sigma_{1,max}$ for the edge of the hole. The differences of the stress magnitudes in the outer paths in the nodes indicated by Angle 1 or 2 and in the nodes indicated by Outer Angle 1 or 2, or Second Outer Angle 1 or 2, are small, and can be considered insignificant to the total magnitudes of the stresses. From this result the conclusion can be drawn, that the angles to the location of $\sigma_{1,max}$ along circular paths around the hole are the same for the same load case, no matter if the paths are right at the edge of the hole, or a few nodes from the edge. Furthermore, from the results in Table 3.2 and from the symbol plots investigated, the conclusion that the crack will grow at an angle perpendicular to the edge of the hole, can be drawn.

Chapter 4

Beam strength calculations by means of three fracture criteria

The shear force capacities of beams with holes was calculated by use of the three fracture mechanics criteria that were defined in Chapter 2. The calculations were performed with the finite element method.

4.1 Beam geometries

The calculations involved 11 differently shaped beams. The geometries of the modeled beams and the load situations that were analyzed were taken from a report by Serrano [14], that contained results from laboratory tests of wooden I-beams manufactured by Swelite. By using the same geometries and load situations, the results from the FE-calculations can be compared with the results from the tests. All beams except two had a depth H of 220 mm. These beams (d203 and d203x275) had instead a depth H of 500 mm. All beams had a web thickness, b_w , of 8 mm, a flange thickness, b_f , of 47 mm and a flange depth, h_f , of 47 mm. The beams had a total length of $11H$ and the free span had a length of $10H$. The distance from the edge of the hole to the left support was H mm as well as the distance between the edges of the holes for the beams with two holes. For the square- and rectangle-shaped holes, the corners were cut with a radius of 20 mm. The types of holes used and their dimensions are included in Table 4.1, where $L = L_1 + L_2$. Figure 4.1 shows the beam geometries and the test setup.

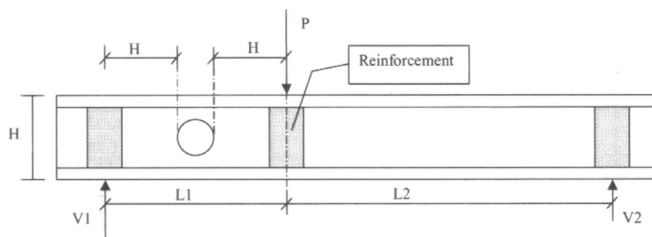


Figure 4.1: *The setup for the previous performed tests [14].*

Table 4.1: *The analyzed beams. H = the height of the beam. d = the diameter of the hole. h = the depth of the square- or rectangle-shaped hole. w = the base of the square- or rectangle-shaped hole.*

Beam	H [mm]	Hole type	No. of holes	d alt. h/w [mm]	L [mm]	L_2 [mm]	L_2/L [-]
d40	220	circular	1	40.0	2200	1720	0.78
d63	220	circular	1	63.0	2200	1697	0.77
d94.5	220	circular	1	94.5	2200	1666	0.76
d126	220	circular	1	126.0	2200	1634	0.74
d203	500	circular	1	203.0	5000	3797	0.76
d2x63	220	circular	2	63.0	2200	1414	0.64
d2x126	220	circular	2	126.0	2200	1288	0.59
d63x126	220	rectangle	1	63.0/126.0	2200	1634	0.74
d126x126	220	square	1	126.0/126.0	2200	1634	0.74
d126x275	220	rectangle	1	126.0/275.0	2200	1485	0.68
d203x275	500	rectangle	1	203.0/275.0	5000	3725	0.75

4.2 Converting point load to shear force

Later in this chapter the fracture loads P_f for beams supported and loaded according to Figure 4.1 will be calculated using the three fracture criteria. When the fracture loads have been calculated, they need to be converted into shear force capacities V_f . This can be achieved by using Equation 4.1.

$$V_1 = P \frac{L_2}{L} \quad (4.1)$$

where V_1 = the shear force caused by the applied point load P and $L = L_1 + L_2$, where L_1 and L_2 are visualized in the Figure 4.1. Table 4.1 shows the lengths L and L_2 and for all beams.

4.3 Summary of results from beam tests

For the tests buckling of the flange was avoided during loading by including transverse supports [14]. For each type of beam seven nominally equal beams were tested and from these tests the average values of the failure load P_f and the shear force capacity V_f were calculated. The results are summarized in Table 4.2, which also includes the standard deviation for each type of beam. For most beams the failure was caused by shear failure at the hole, though for some beams (d2x63, d2x126 and d126x126) failure was caused by a combination of shear failure at the hole and failure at the flanges. The test study did not include investigation of the location and direction of cracks around the hole.

Table 4.2: Average maximum point load P_f , average shear force capacity V_f and standard deviation from tests.

Beam	P_f [kN]	V_f [kN]	<i>Std.dev.</i> [kN]
d40	28.2	22.0	2.1
d63	21.4	16.5	2.0
d94.5	16.0	12.1	0.8
d126	16.3	12.1	0.8
d203	33.2	25.2	1.0
d2x63	26.9	17.3	0.4
d2x126	20.0	11.7	1.1
d63x126	16.2	12.1	0.7
d126x126	14.1	10.4	0.7
d126x275	10.3	7.0	0.4
d203x275	16.2	12.1	0.9

4.4 Finite Element calculations

The beam geometries are described in Table 4.1 above. A distributed load with a magnitude of 1 N/mm^2 was applied to the beams at the position indicated by Figure 4.1. It was distributed over an area of $50 \times 47 \text{ mm}^2$, hence, the applied load, P , was 2.350 kN. The beams were modeled in ABAQUS, with the material properties described in Chapter 2 and with the same type of elements as the beams of Chapter 3.

To imitate the boundary conditions and the applied load of the tests, a length of 50 mm at each support was constrained in all directions to a single point in the middle of this length, with coupling constraints. For the left support the movement in this single point was then constrained to zero in the x - and y -direction, like a fixed support, and for the right support the motion in the center point was constrained to zero in the y -direction, consistent with a roller support.

The beams were meshed in a similar manner as the beams in Chapter 3. For the beams with a hole diameter d equal to the total depth of the web h_w , triangular elements were used in the area around the top and the bottom of the hole, where the web area was very small. The partitioning and the meshes were similar to those in Figure 3.2 and 3.3.

4.5 Location and growth direction for cracks

Before calculating the shear force capacities for the beams, the locations of the maximum of the first principal stress $\sigma_{1,max}$ around the holes were calculated. For each hole Angle 1 and Angle 2 (see Figure 3.5) from the center of the hole to $\sigma_{1,max}$ at the edge of the hole for the upper part and the lower part of the hole are shown in Table 4.3 below. All assumed cracks used in the calculations in the rest of this chapter will initiate at the edge of the hole at the point where $\sigma_{1,max}$ occurs for the upper or for the lower half of the hole. In line with the results from Chapter 3, the cracks are then assumed to grow in a direction perpendicular to the edge of the hole. For each of the three criteria used, an assumption has to be made about in which part of the beam, at the upper part of the hole or at the lower part of the hole, the crack will initiate and grow. For each criteria the part which gave the lowest values of the calculated shear force capacity was used. The chosen part for each criteria is discussed in their respective section below.

Table 4.3: *The angles describing the locations of the maximum principal stresses at the upper and lower edge of the hole.*

Beam	Left hole		Right hole	
	Angle 1 [°]	Angle 2 [°]	Angle 1 [°]	Angle 2 [°]
d40	44.02	45.00	-	-
d63	42.19	45.00	-	-
d94.5	42.80	47.19	-	-
d126	41.33	45.92	-	-
d203	41.82	49.09	-	-
d2x63	43.59	46.41	40.78	47.81
d2x126	42.05	45.92	38.57	49.59
d63x126	47.44	52.09	-	-
d126x126	34.99	44.98	-	-
d126x275	45.00	47.81	-	-
d203x275	47.74	47.74	-	-

4.6 The point stress criterion

4.6.1 Method

The shear force capacity was calculated with the point stress criterion by use of the failure criterion $\sigma_{1,max} = f_t$ (see Section 2.4.1), where $f_t = 30.0$ MPa (see Section 2.5) and by determining the first principal stress σ_1 in the nodes at the edge of the hole. The largest of these stresses, $\sigma_{1,max}$ were used to calculate the failure loads P_f for the beams as mentioned in Chapter 2. From these failure loads the shear force capacities V_f for the beams could be calculated.

4.6.2 Results

In Table 4.4 the results from the use of the point stress criterion are shown. The bold numbers indicate the part around the hole that had the largest of the two $\sigma_{1,max}$ and thus the value of $\sigma_{1,max}$ that is used when calculating the failure load P_f . Figure 4.2 below shows the difference between the test results in the previous study [14], and the results from using the point stress criterion for the different beams.

Table 4.4: *The results from the use of the point stress criterion.*

Beam	$\sigma_{1,max}$ for the load P [MPa]				P_f [kN]	V_f [kN]
	Left hole		Right hole			
	Upper part	Lower part	Upper part	Lower part		
d40	5.54	5.52	-	-	12.73	9.95
d63	5.84	5.84	-	-	12.07	9.31
d94.5	6.49	6.51	-	-	10.83	8.20
d126	7.13	7.12	-	-	9.88	7.34
d203	2.79	2.81	-	-	25.13	19.08
d2x63	4.97	4.88	4.90	4.99	14.13	9.08
d2x126	5.72	5.61	5.66	5.90	11.96	7.00
d63x126	9.50	9.74	-	-	7.24	5.38
d126x126	12.03	12.57	-	-	5.61	4.17
d126x275	17.26	18.15	-	-	3.88	2.62
d203x275	7.48	7.48	-	-	9.43	7.02

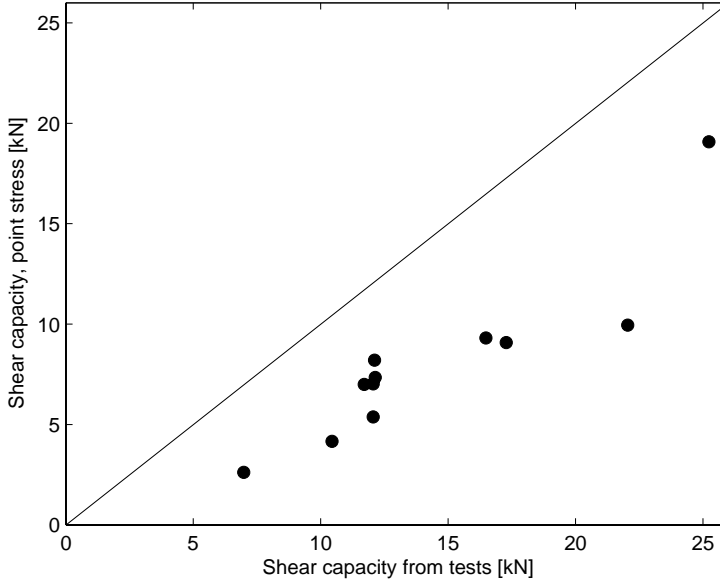


Figure 4.2: *The relationship between the shear force capacity from tests and the shear force capacity obtained by the point stress criterion.*

4.7 The mean stress criterion

4.7.1 Method

The length x_0 , over which to calculate the mean stress $\sigma_{1,mean}$ is determined with the use of the material parameters from Section 2.5 and Equation 2.13.

$$x_0 = \frac{2 EG_f}{\pi f_t^2} = \frac{2}{\pi} \cdot \frac{5748 \cdot 10^6 \cdot 3494}{(30 \cdot 10^6)^2} = 0.0142 \text{ m} = 14.2 \text{ mm} \quad (4.2)$$

For all beams except two, d126x126 and d126x275, the length x_0 fitted within the web. The first principal stress σ_1 along the assumed crack path was calculated and the mean stress over this path, $\sigma_{1,mean}$, was determined by first integrating σ_1 over the distance x_0 from the edge and then dividing the integration with the respective distance from the edge of the hole, in accordance with Equation 4.3.

$$\sigma_{1,mean} = \frac{1}{x_0} \int_0^{x_0} \sigma_1 dx \quad (4.3)$$

This mean stress is then used to calculate the failure load P_f in accordance with Chapter 2. The failure load P_f is then converted into the shear force capacity V_f . Fracture occurs when $\sigma_{1,mean} = f_t$.

4.7.2 Results

The figures in Appendix B show the relationship between the distance x from the edge of the hole and the mean stress calculated over this distance. In Table 4.5 below the results from the use of the mean stress criterion and the choice of crack location are shown. The bold numbers indicate in which part the largest of the two maximum mean stresses $\sigma_{1,mean}$ at distance x_0 occurs, and thus the values used for calculating the failure loads. Notice that for four beams the bold numbers do not indicate the same part as did the point stress criterion, since the chosen assumed crack location is in the part with the maximum mean stress $\sigma_{1,mean}$ at distance x_0 , which may not necessarily be on the same side of the hole as the largest of the two maximum stresses $\sigma_{1,max}$ found in Section 4.6 (see discussion in Section 4.7.3).

The differences between the shear force capacities gained from using the mean stress criterion and from the tests are shown in Figure 4.3. All values of the shear force capacity with the mean stress criterion are lower than those from the tests.

Table 4.5: *The shear force capacity V_f with the mean stress criterion. The bold numbers indicate in which part around the hole the largest of the two $\sigma_{1,mean}$ over the specific distance x_0 occurs, and thus the value used in the calculations.*

Beam	$\sigma_{1,mean}$ for the load P [MPa]				P_f [kN]	V_f [kN]
	Left hole		Right hole			
	Upper part	Lower part	Upper part	Lower part		
d40	2.84	2.96	-	-	23.82	18.62
d63	3.53	3.68	-	-	19.18	14.79
d94.5	4.37	4.58	-	-	15.44	11.69
d126	5.06	5.20	-	-	13.57	10.08
d203	2.27	2.38	-	-	29.57	22.46
d2x63	3.01	3.07	2.89	3.22	21.89	14.07
d2x126	4.05	4.10	3.92	4.40	16.03	9.39
d63x126	5.28	5.59	-	-	12.60	9.36
d126x126	6.65	8.84	-	-	7.97	5.92
d126x275	11.54	12.47	-	-	5.65	3.82
d203x275	4.43	4.83	-	-	14.60	10.87

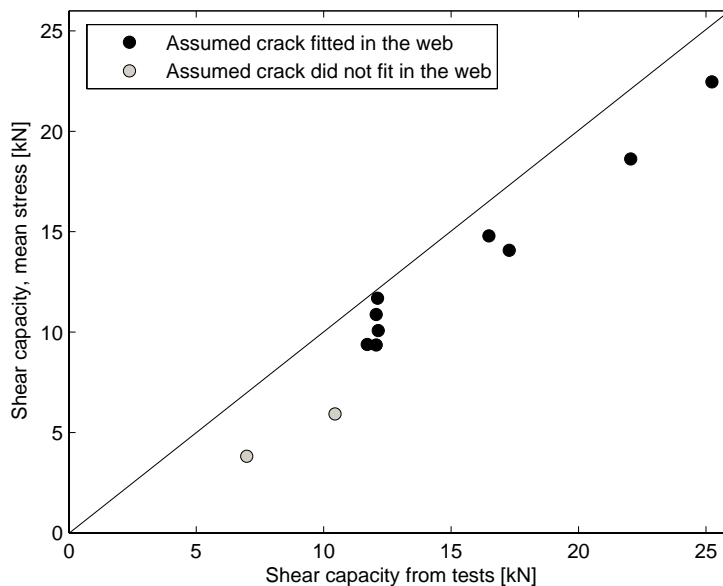


Figure 4.3: *The relationship between V_f from tests and V_f with the mean stress criterion, when assuming that the crack will occur in the part with the maximum $\sigma_{1,mean}$ over the distance x_0 .*

4.7.3 Discussion

Calculations were performed for both an assumed crack in the upper part of the hole and in the lower part. For both these parts the crack was assumed to initiate in the node with the maximum of the first principal stress $\sigma_{1,max}$ for the respective part. The mean stress plots for cracks in the upper and the lower part differ somewhat and the largest $\sigma_{1,mean}$ along the distance x_0 of the two are not always at the same part of the hole as the location of $\sigma_{1,max}$ around the hole, as would have been expected. Hence, a decision considering in which part the assumed crack will initiate had to be made, and the option was between the part with the largest $\sigma_{1,max}$ at the edge of the hole, and the part with the largest $\sigma_{1,mean}$ at distance x_0 from the hole, starting at the node with $\sigma_{1,max}$ for that part. These two options only result in use of different parts for the location of the assumed crack for four of the beams, and the differences in the shear force capacity V_f that this causes are illustrated in Figure 4.4.

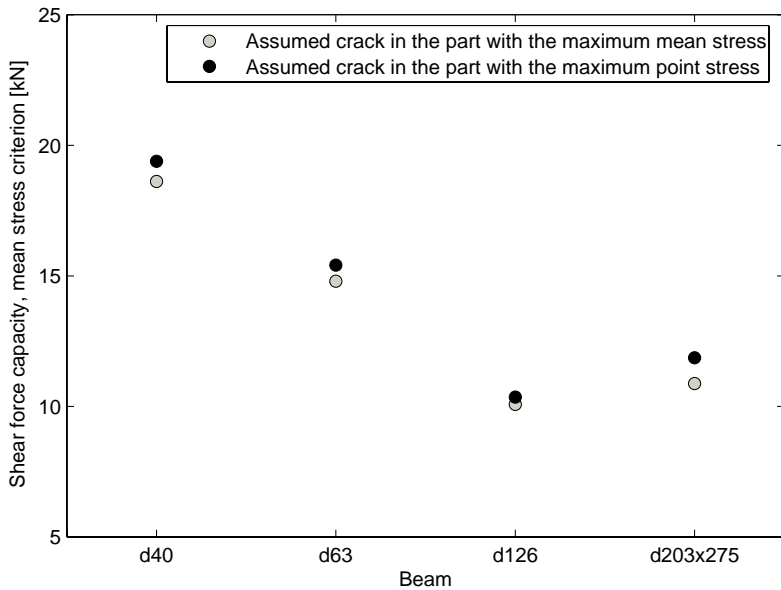


Figure 4.4: *The difference in shear force capacity from using different locations for the assumed crack.*

The differences between the shear force capacities V_f from the two alternative crack positions are small and since the use of the location of the maximum $\sigma_{1,mean}$ over length x_0 gives slightly lower values for the shear capacity, this can be considered the safe choice, and is therefore used in the remaining of this chapter.

4.8 The initial crack criterion

4.8.1 Method

When using the initial crack criterion to calculate the shear force capacity, the energy release rate G for crack growth can be expressed by Equation 2.17, repeated in Equation 4.4.

$$G = \frac{\partial W}{b_w \partial a} \quad (4.4)$$

First, each beam was modeled with an initial crack with the length $a_0 = x_0/2$, as described in Section 2.4.3. This was performed in ABAQUS by drawing the crack with a partitioning tool, and then assigning a crack along this partition. This

resulted in double nodes along the line. For the lower part of the hole for beam d126x275 the length a_0 did not fit into the web. Instead the longest possible length in the same direction that fitted within the web was used. The cracks for all beams initiated in the node with the maximum of the first principal stress $\sigma_{1,max}$ at the edge of the hole in the upper or lower part, and grew in the direction perpendicular to the edge of the hole. For this first crack the external work W_1 was calculated and then one node at the tip of the crack was opened to simulate crack growth. This resulted in a new crack with length $a_0 + 2x_a$. The external work W_2 for the new crack was calculated, as well as the growth length Δa for the crack (see Section 2.4.3 and Figure 2.6). These values were then used to calculate the energy release rate G for each beam with crack lengths according to Table 4.6 and from the specific applied load P :

$$G \approx \frac{\Delta W}{b_w \Delta a} = \frac{W_2 - W_1}{b_w(a_0 + 2x_a - a_0)} \quad (4.5)$$

To calculate the failure load P_f the critical value of the energy release rate G_f was used ($G_f = 3494 \text{ J/m}^2$ as mentioned in Section 2.5):

$$G_f = G\left(\frac{P_f^2}{P^2}\right) \Rightarrow P_f = P \sqrt{\frac{G_f}{G}} \quad (4.6)$$

All alternative positions for the cracks, which are the upper and lower part of the hole and also the right or the left hole for the cases with two holes, were modeled and tested in ABAQUS.

4.8.2 Results

The results are shown in Table 4.6. The bold areas indicate the part with the largest of the two $\sigma_{1,max}$ at the edge of the hole, one occurring at each side of the hole. The non-bold areas can be considered as alternatives to this area for the location of the modeled crack. The relation between the shear force capacity V_f from the previous tests and from the use of the initial crack criterion (the bold areas) is shown in Figure 4.5.

Table 4.6: *The shear force capacity with the initial crack criterion. The bold areas indicate where around the hole the maximum of the first principal stress $\sigma_{1,max}$ for the load P occurs, and thus the values used for calculation the shear force capacity V_f .*

Beam	Location	a_0 [mm]	$a_0 + 2x_a$ [mm]	ΔW [J]	G for load P [J/m ²]	P_f [kN]	V_f [kN]
d40	upper part	7.1	8.1	0.31	38.75	22.32	17.45
d40	lower part	7.1	8.1	0.33	41.25	21.63	16.91
d63	upper part	7.1	8.1	0.52	65.00	17.23	13.29
d63	lower part	7.1	8.1	0.50	62.50	17.57	12.55
d94.5	upper part	7.1	8.1	0.78	97.50	14.07	10.65
d94.5	lower part	7.1	8.1	0.88	110.00	13.24	10.03
d126	upper part	7.1	8.1	1.15	143.75	11.59	8.61
d126	lower part	7.1	8.1	1.15	143.75	11.59	8.61
d203	upper part	7.1	8.1	0.21	26.25	27.11	20.59
d203	lower part	7.1	8.1	0.23	28.75	29.91	19.67
d2x63	upper right part	7.1	8.1	0.37	46.25	20.43	13.13
d2x63	lower right part	7.1	8.1	0.43	53.75	18.95	12.18
d2x63	upper left part	7.1	8.1	0.34	42.50	21.31	13.70
d2x63	lower left part	7.1	8.1	0.37	46.25	20.43	13.13
d2x126	upper right part	7.1	8.1	0.69	86.25	14.96	8.76
d2x126	lower right part	7.1	8.1	0.84	105.00	13.56	7.94
d2x126	upper left part	7.1	8.1	0.71	88.75	14.75	8.63
d2x126	lower left part	7.1	8.1	0.75	93.75	14.35	8.40
d63x126	upper part	7.1	8.1	1.18	147.50	11.44	8.50
d63x126	lower part	7.1	8.1	1.29	161.25	10.94	8.13
d126x126	upper part	7.1	8.1	1.72	215.00	9.47	7.04
d126x126	lower part	7.1	8.1	1.52	190.00	10.08	7.49
d126x275	upper part	7.1	8.1	2.39	298.75	8.04	5.43
d126x275	lower part	5.5	6.5	3.25	406.25	6.89	4.65
d203x275	upper part	7.1	8.1	0.86	107.50	13.40	9.98
d203x275	lower part	7.1	8.1	1.00	125.00	12.42	9.26

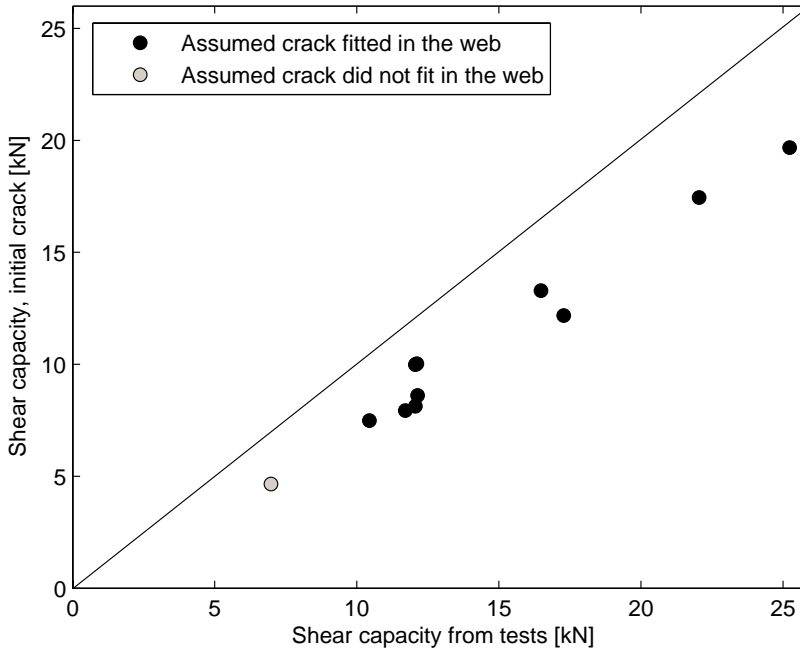


Figure 4.5: *The relation between the shear force capacity from tests and from the use of the initial crack criterion, for cracks initiating in the node with the maximum of the first principal stress.*

4.8.3 Discussion

As for the mean stress criterion, the location of the assumed crack has to be decided upon. It is also of interest to investigate if the choice between these alternative crack locations has any significant impact on the shear force capacity. For most cases, but not for all, the shear force capacity is larger in the area with the maximum point stress at the edge of the hole, compared with alternative locations for the crack. However, the difference is not large. The differences between the shear force capacities calculated for the bold areas and for the alternative non-bold areas are shown in Figure 4.6. Since the use of the position where the maximum point stress at the edge of the hole occurs gives slightly lower values of the shear force capacity for most beams, this position was used. For beam d126x275 the lengths a_0 and $a_0 + 2x_a$ did not fit into the web on the lower side of the hole, and were therefore instead set to 5.5 and 6.5 mm, respectively. This side of the beam gave a lower value for the failure load P_f than the the upper side of the beam, and therefore it was used.

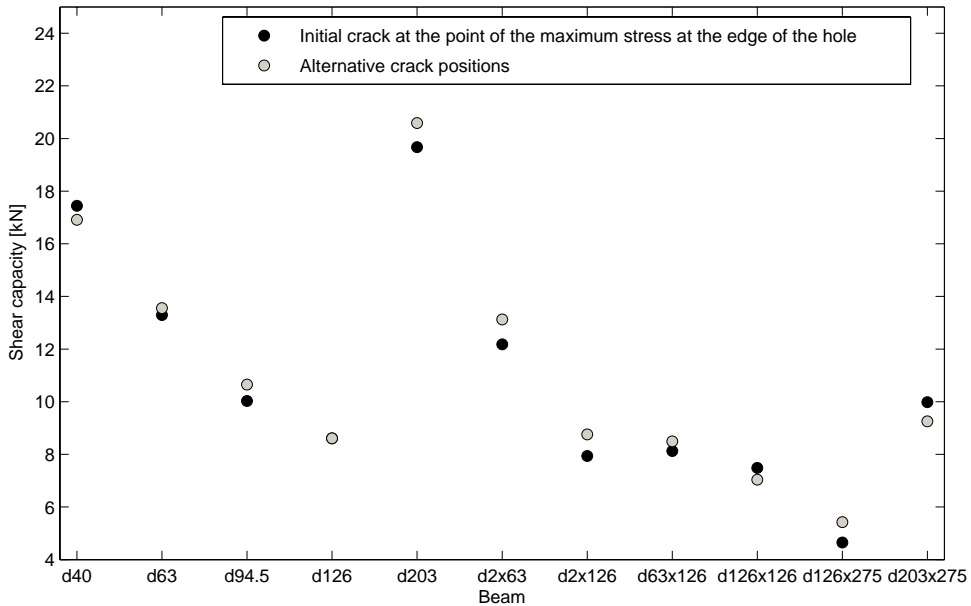


Figure 4.6: *The influence from the location of the initial crack on the shear force capacity. The options for the locations are between the part with the total maximum point stress at the edge of the hole, or at the point with the local maximum point stress.*

4.9 Cracks that do not fit into the web

With the mean stress criterion the distances x_0 over which to calculate the mean stress did not fit into the web for all models. This problem occurred when the depth of the hole had the same magnitude as the total web depth for the rectangular holes. However, these holes are not accepted neither by Swelite's nor Forestia's recommendations. Rectangular holes of this size are not common, and because of this and since they are not recommended by the manufacturers, it is not considered as a major problem if x_0 does not fit into the web for these beams. However, a short discussion regarding calculation solutions when this occurs is motivated.

For the beams where x_0 did not fit into the web for the mean stress criterion, the calculations in Section 4.7 were performed with the longest possible distance that fitted into the web in the crack direction, hence, the distance from the edge of the hole to the web to flange-joint in the chosen direction. This shorter x_0 resulted in lower values on the failure load and thus a lower shear force capacity, than if the original x_0 would have fitted into the web. One option for calculating the shear force capacity with the mean stress criterion when x_0 does not fit into the web is thus to

use the longest possible values for x_0 for these beams instead. This will however not represent the actual shear force capacity accurately.

For the point stress criterion this problem does not exist, since the shear force capacity is calculated for the maximum of the first principal stress $\sigma_{1,max}$ in one single node. Another alternative for calculating the shear force capacity for the beams where x_0 did not fit into the web is therefore to use the point stress criterion instead of the mean stress criterion. This is a relatively easy way to estimate the shear force capacity V_f , and since the point stress criterion gives lower values on the shear force capacity than the mean stress criterion, this will give value on the safe side.

Yet another alternative would be to use the initial crack criterion for these models. Since the assumed crack length will be maximum $x_0/2$ plus the length of an element side, this crack is more likely to fit within the web, and the extent of this problem will thus be reduced. In the calculations in Section 4.8 the assumed crack a_0 did not fit into the web for the lower side of the model d126x275. When this occurred the calculations were instead performed with the longest possible crack. Since the original assumed crack a_0 was half the size of x_0 , the difference that the shorter a_0 makes is smaller, than the difference a shorter x_0 makes. The use of the initial crack criterion for the models where the original x_0 does not fit into the web can thus be motivated, but the calculations with the initial crack criterion are far more complicated.

Another option is to still use the mean stress criterion, but manipulating the σ_{mean}/x plots (see Appendix B) and thus gain a value for the distance x_0 , though somewhat modified. When calculating the mean stress over the distance x , first of all the maximum stress at the distance x is calculated. With this modified mean stress method, the maximum stress plots is elongated by dragging the lowest value horizontally, and thus setting the maximum stress at all following distances from the edge of the hole to the value at the longest possible distance in the web from the edge along the assumed crack path. This modified plot is then integrated and each value of the stress is divided by the distance x , just as in previous calculations.

Chapter 5

Evaluation and new calculation method

5.1 Evaluation of the calculation criteria

Figure 5.1 below shows a comparison between the three criteria used in the calculations and the results from the tests. The figure also includes the relationship between the characteristic shear capacity, V_k , from tests and from using Swelite's equation, see Section 2.2.2.

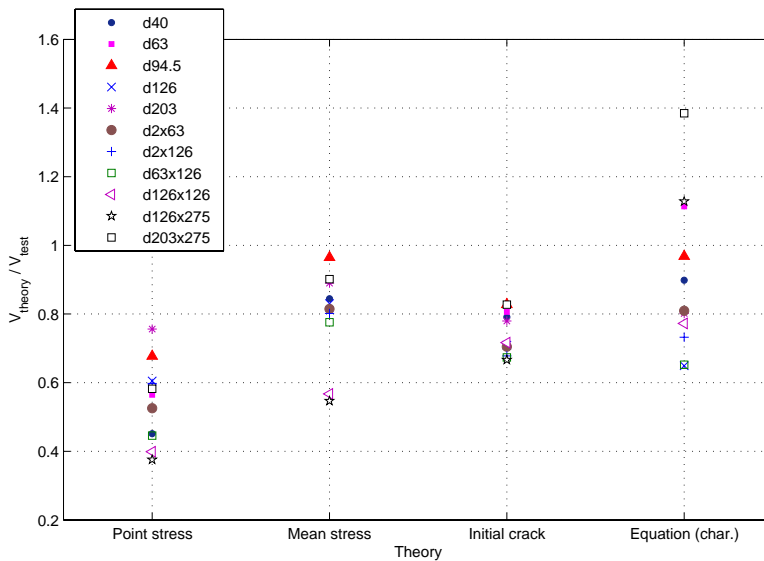


Figure 5.1: *The ratio V_{theory}/V_{test} for the three criteria used and from Swelite's equation. For the equation, the characteristic values for both the theory and the tests have been used.*

Since the material used in the models may not correspond to the material used in the previous tests, the ratio between the largest and smallest V_{theory}/V_{test} for the different theories is of interest, and not how close V_{theory}/V_{test} is to 1.

With the exception of the two models d126x126 and d126x275, for which the crack length x_0 did not fit into the web, the use of the mean stress criterion gave a small ratio of approximately $0.96/0.78 = 1.23$ for V_{theory}/V_{test} . The initial crack criterion also gave a small V_{theory}/V_{test} ratio, approximately $0.83/0.68 = 1.22$. The point stress criterion gives the highest value of the same ratio among the three criteria, approximately $0.76/0.38 = 2.00$. The equation gave the largest V_{theory}/V_{test} ratio, approximately $1.39/0.65 = 2.14$ and can thus be considered as not a suitable way of calculating the reduced shear force capacity for a beam with a hole in the web, especially since three of these characteristic values are lower than the corresponding characteristic values from the tests (see Section 5.2).

If only taking the cases for which the assumed crack fitted within the web into consideration, the mean stress criterion or the initial crack criterion are obviously the best choices for estimating the beams' shear force capacity. Figure 5.2 shows the calculated shear force capacities from the use of the three criteria and from the tests. The figure shows that the point stress criterion gives values of the shear force capacity that heavily differs from the shear force capacity from the tests, especially for the smaller holes. For the beam d40 with a hole diameter of 40 mm, the calculated shear force capacity from using the point stress criterion is less than half of the shear force capacity from tests. The point stress criterion is thus severely underestimating the true shear force capacity for that beam.

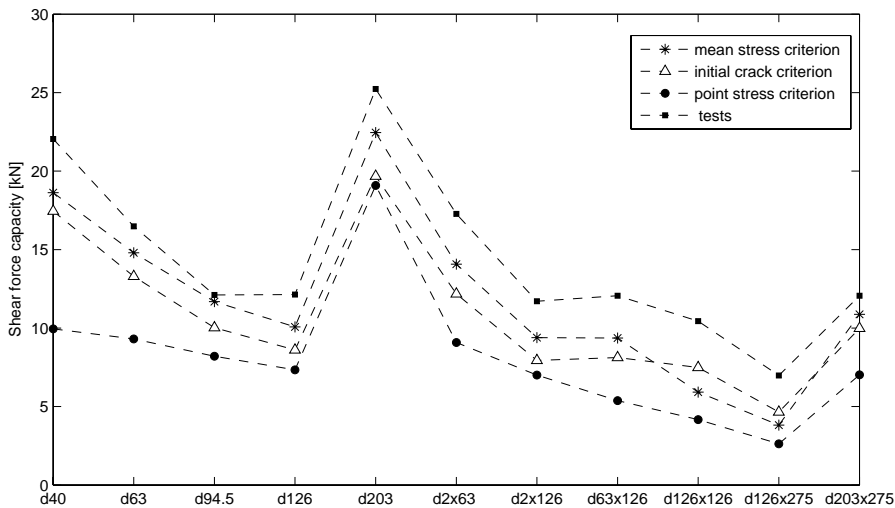


Figure 5.2: The shear force capacity calculated with the three criteria and from the tests.

Another way to visualize the difference in the shear force capacity between the three criteria is to summarize the Figures 4.2, 4.3 and 4.5 into Figure 5.3.

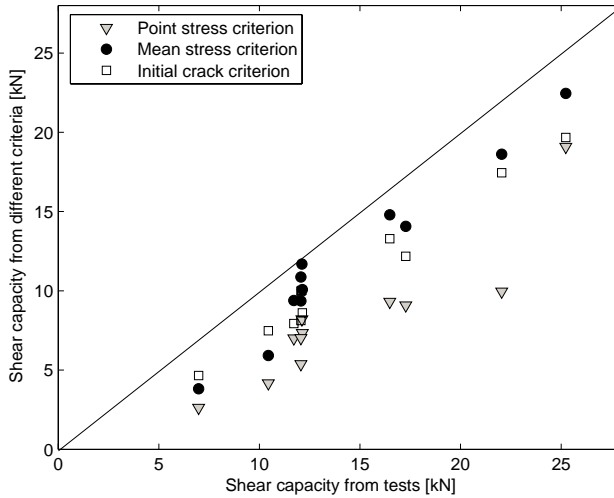


Figure 5.3: *The relation between the shear force capacity from the tests and the shear force capacity with the three criteria.*

From the figures in this section it is clear that among the three criteria, the mean stress criterion or the initial crack criterion are to be preferred, since the point stress criterion gives the largest span on the ratio V_{theory}/V_{test} . A small span would indicate that the theory could be used for calculating the reduced shear force capacity without severely underestimating the strength of some beams. From the figures it is also clear that the mean stress criterion and the initial crack criterion gave fairly similar results. However, the mean stress criterion is a far more easy method to use, since no actual crack need to be modeled. For the initial crack criterion, two calculations are also needed for each beam to obtain W_1 and W_2 , while the mean stress criterion only needs one calculation for each beam. The initial crack criterion is hence far more time consuming than the mean stress criterion. One advantage with the initial crack criterion is however that the problem with cracks that do not fit into the web will not occur to the same extent as it does for the mean stress criterion, as mentioned in Section 4.9.

5.2 Evaluation of current calculation method

5.2.1 Method

The calculation method used by Swelite and Forestia, for calculating the reduced shear force capacity for I-beams with holes in the web was mentioned in Section 2.2 and the equations used will be repeated here for convenience.

$$V_{k,hole} = V_k \cdot k \quad (5.1)$$

$$k = \frac{H - h_f - 0.9d}{H - h_f} \quad (5.2)$$

The reduced characteristic shear capacity, $V_{k,hole}$, is calculated from the characteristic shear capacity for the beam without any hole, V_k , by multiplying it with the reduction factor k . The factor k is based on the total beam depth H , the depth of the flanges, h_f , and the diameter of the hole, d .

In the study that contained the results from the test [14], that have been used for comparison throughout this thesis, the shear force capacities for the tested beams were compared to the shear force capacities from the equations. For this comparison, the mean values of the shear force capacities from the tests for each type of beam were converted into the characteristic shear force capacities $V_{k,test}$, by use of the standard deviation. These values were compared to the characteristic shear force capacities calculated with Equation 5.1 and Equation 5.2 using the characteristic shear force capacity for a beam of type H 220 without any hole, V_k , given by Swelite [15].

5.2.2 Results

Figure 5.4 shows the comparison between the characteristic shear force capacities from the tests, $V_{k,test}$ and the characteristic shear force capacities from the use of the equations recommended by Swelite and Forestia, $V_{k,hole}$.

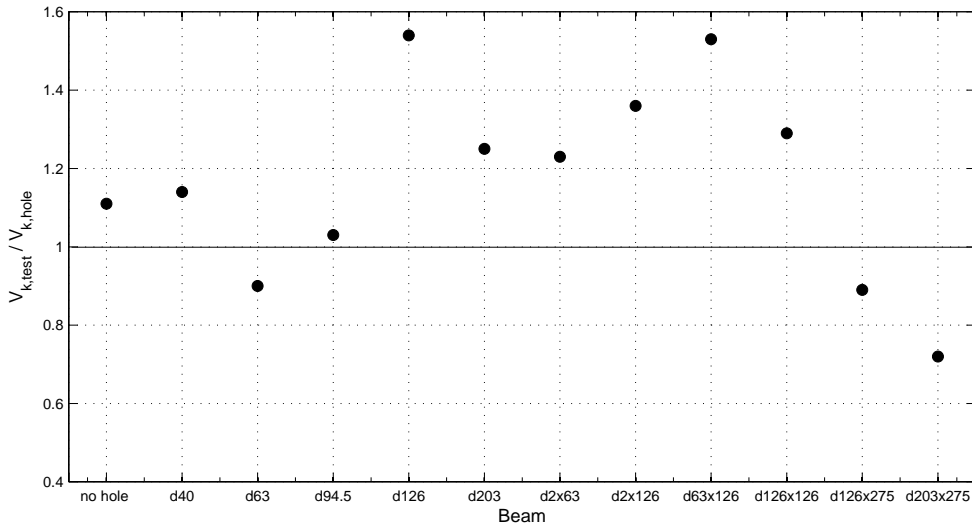


Figure 5.4: The ratio between the characteristic shear force capacity from the tests, $V_{k,test}$ and from the equations, $V_{k,hole}$.

5.2.3 Discussion

From Figure 5.4 it is clear that for three beams the characteristic shear force capacity from the tests, $V_{k,test}$, was lower than the characteristic shear force capacity from the equations, $V_{k,equ}$. Since the beams used in the test were manufactured by Swelite (at the time named Masonite AB) [14], and are thus comparable with the results from the equations, it is obvious that Equation 5.1 and Equation 5.2 are not suitable for calculating the reduced shear force capacity for all beams used. The beams that had a ratio $V_{k,test}/V_{k,equ}$ smaller than 1 was d63, d126x275 and d203x275. The beams d126x275 and d203x275 do not fulfill Swelite's or Forestia's recommended dimensions (Section 2.2), however, the beam d63 fulfills the requirements from both manufacturers, and one would therefore expect that the shear force capacity from the tests for this beam would be larger than the calculated reduced shear force capacity, which is not the case.

From Figure 5.4 it is also clear that for some beams the calculation method from Swelite and Forestia severely underestimates the shear force capacity. For example, the ratio $V_{k,test}/V_{k,equ}$ is almost 1.6 for the beams d126 and d63x126 and almost 1.4 for the beam d2x126. From 5.4 and Figure 5.1 the conclusion can be drawn that the method recommended by Swelite and Forestia for calculating the reduced shear force capacity is not very suitable, and efforts to develop a new calculation method based on fracture mechanics are motivated.

5.3 Beam parameter study

The parameter study was based on the mean stress criterion, since this method resulted in a short span for the ratio V_{theory}/V_{test} , and since this is a fairly easy method to use, as was discussed in Section 5.1. The parameters investigated are the material parameters E , G_f and f_t . The reason for this additional parameter study is that the values of these parameters in the previous tests are not known. Because of this the used values of these parameters in the calculations in Chapter 4 may not be near the values for the real beams used in the test. Therefore it is of interest to investigate how much a change in these values influence the calculations.

5.3.1 Method

The influence from the Young's modulus E , the fracture energy G_f and the tensile strength f_t on the shear force capacity V_f was investigated. A change in any of these parameters will result in a change in the distance x_0 , over which to calculate the mean stress, and thus a change in the magnitude of the failure load P_f and ultimately the shear force capacity V_f . By including these material parameters in a dimensionless value X , see Equation 5.3, they can be compared to the shear force capacity for different beams with a span of tensile strengths.

$$X = \frac{h_w}{\frac{EG_f}{f_t^2}} \quad (5.3)$$

where h_w is the depth of the web.

The span of X includes variations of E between 3 000 MPa and 16 000 MPa, with all other values kept constant and given by Chapter 2. By instead changing only G_f instead of E , G_f will vary between 1900 J/m² and 10 000 J/m². By changing only f_t , f_t will vary between 18 and 41 MPa. For some beams which had a diameter of the hole of the same magnitude as the depth of the web, this could not be calculated, since the assumed crack lengths did not fit into the web. The beams for which x_0 in Chapter 4 did not fit into the web were therefore excluded from the calculations in this parameter study. The value X for the previously mentioned span was plotted against Y , see Equation 5.4, which included the shear force capacity of the beam V_f , the thickness of the web b_w , the depth of the web h_w and the tensile strength of the web material, f_t .

$$Y = \frac{V_f}{b_w h_w f_t} \quad (5.4)$$

5.3.2 Results

For all the 11 beams studied lower part of the hole will require a lower load for fracture to initiate, and it is therefore reasonable to focus only on assumed cracks in the lower part of the beams.

Figure 5.5 shows the relationship between X and Y for the beam depth 220 mm, and thus the influence from different material parameters on the resulting shear force capacity V_f . By using Figure 5.5 the shear force capacity for beams with the same geometries and various isotropic web materials can be estimated.

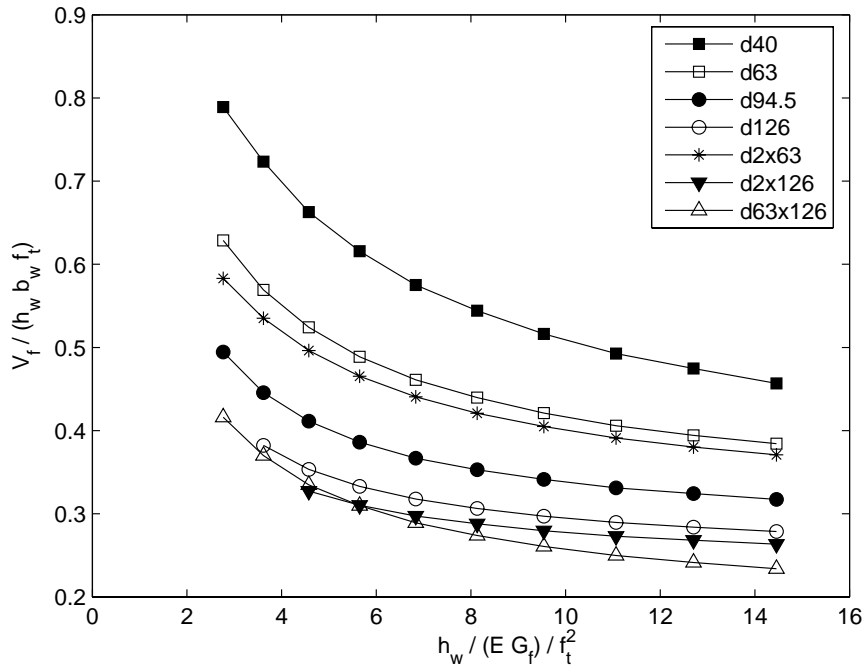


Figure 5.5: The influence of the material parameters E , G_f and f_t on the shear force capacity V_f of different beams with depth of 220 mm.

Figure 5.6 shows the relationship between X and Y for the beams with a depth H of 500 mm. Figure 5.7 shows Figure 5.5 and Figure 5.6 combined in one figure. Since the depth H is included in the X variable the X -axis will not have the same limits for the two figures 5.5 and 5.6.

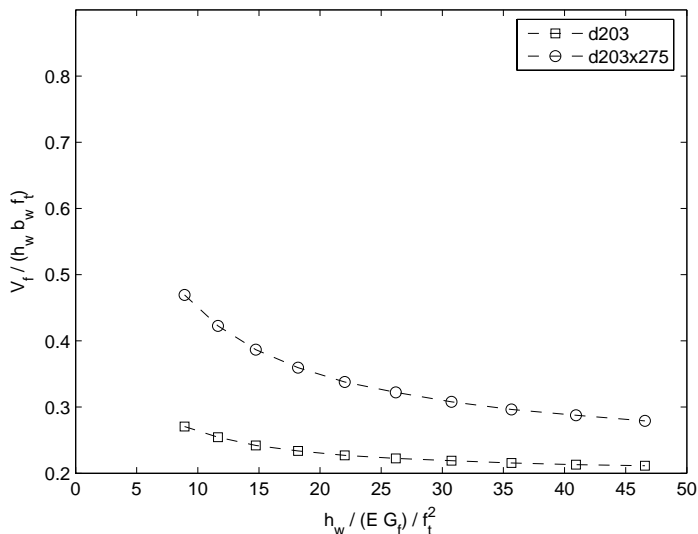


Figure 5.6: The influence of the material parameters E , G_f and f_t on the shear force capacity V_f of beams with the depth 500 mm.

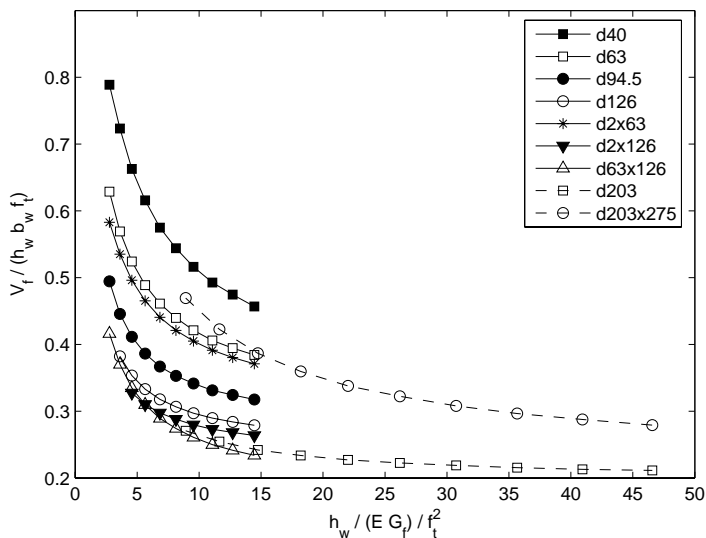


Figure 5.7: The influence of the material parameters E , G_f and f_t on the shear force capacity V_f of different beams.

5.4 New approximate strength equation

Since the shear strength equation recommended by Swelite and Forestia was found to be poor earlier in this chapter a new approximate equation for simple calculation of the reduced shear force capacity for beams with holes in the web will be suggested and discussed. In the evaluation of the fracture mechanics theories in Section 5.1 the mean stress criterion and the initial crack criterion were found to be suitable for calculating the shear force capacities of beams with holes in the web. However, the mean stress criterion is easier to use than the initial crack criterion, and therefore a new recommended method would be to use the mean stress criterion. A new calculation method could be based on the plots obtained in the parameter study performed in Section 5.3, see Figure 5.7, since these plots are based on the mean stress criterion. By using Figure 5.7 for beams with similar geometries and hole diameters as the tested beams, the shear force capacity $V_{k,hole}$ for I-beams with various isotropic web materials can be read from the plot, if the material parameters are known. Note however, that these plots have only been performed for a few beams, and further research is needed to obtain more general plots. Furthermore, the plots are only valid for the current load situation (see Figure 4.1), and this load situation does not only result in a shear force acting in the hole, but also a bending moment.

Another way to use the mean stress criterion as a base for calculating $V_{k,hole}$ is to use an equation fitted to the plots in Figure 5.7. This was performed for the beams with one circular hole by applying a function with five unknown coefficients, shown in Equation 5.5, where $A1$, $A2$, $A3$, $A4$ and $A5$ are the unknown coefficients.

$$\frac{V_{k,hole}}{h_w b_w f_t} = (A1 - A2(\frac{d}{h_w}) + A2(\frac{d}{h_w})^2 + A4(\frac{h_f^2}{b_w l_1}))(\frac{h_w}{EG_f/f_t^2})^{A5} \quad (5.5)$$

where $V_{k,hole}$ = the shear force capacity, h_w = the depth of the web, b_w = the thickness of the web, f_t = the tensile strength of the web material, d = the diameter of the hole, h_f = the depth of the flange, l_f = the moment arm (220 mm for the beam with depth 220 mm and 500 mm for the beam with depth 500 mm), E = Young's modulus for the web material, G_f = the fracture energy of the web material.

The coefficients $A1 - A5$ were determined by means of the least square method. The shear strength according to Equation 5.5 is fitted to the shear strength values of the mean stress method by minimizing the square of the deviation in shear strength. More exactly, the coefficients $A1 - A5$ are chosen so that the least square function $Q = Q(A1, A2, A3, A4, A5)$ is minimized:

$$Q = \sum_{i=1}^5 \sum_{j=1}^{10} (Y(i_j, X_{i,j}) - (A1 - A2(\frac{d}{h_w}) + A2(\frac{d}{h_w})^2 + A4(\frac{h_f^2}{b_w l_1}))(\frac{h_w}{EG_f/f_t^2})^{A5})^2 \quad (5.6)$$

where $Y(i_j, X_{i,j})$ is the shear strength value $V_{k,hole}/(h_w b_w f_t)$ according to the mean stress criterion for beams of type i at value X ($h_w/EG_f/f_t^2$).

The five types of beams considered in the least square curve fitting were d40, d63, d94.5, d126 and d203. These beams are the beams with a single circular hole. For each type of beam ten values of ($h_w/EG_f/f_t^2$) were considered. For $i=1, 2, 3$ and 4, i. e. for beams of types d40, d63, d94.5 and d126 these ten values were:

$$[2.7667 \quad 3.6137 \quad 4.5736 \quad 5.6464 \quad 6.8322 \quad 8.1308 \quad 9.5425 \quad 11.0670 \quad 12.7045 \quad 14.4548]$$

and for $i=5$, i. e. for the beams of type d203, the ten values were:

$$[8.9151 \quad 11.6442 \quad 14.7372 \quad 18.1940 \quad 22.0148 \quad 26.1994 \quad 30.7479 \quad 35.6603 \quad 40.9366 \quad 46.5767]$$

The corresponding $5 \cdot 10 = 50$ values of $Y(i_j, X_{i,j})$ were taken from the parameter study (see Figure 5.7):

$$Y(i_j, X_{i,j}) = \begin{bmatrix} 0.7890 & 0.7233 & 0.6628 & 0.6158 & 0.5750 & 0.5441 & 0.5163 & 0.4926 & 0.4747 & 0.4568 \\ 0.6288 & 0.5691 & 0.5243 & 0.4887 & 0.4611 & 0.4397 & 0.4212 & 0.4059 & 0.3944 & 0.3843 \\ 0.4944 & 0.4457 & 0.4114 & 0.3862 & 0.3669 & 0.3530 & 0.3414 & 0.3311 & 0.3244 & 0.3174 \\ - & 0.3822 & 0.3534 & 0.3330 & 0.3177 & 0.3065 & 0.2970 & 0.2896 & 0.2839 & 0.2788 \\ 0.2707 & 0.2544 & 0.2420 & 0.2338 & 0.2270 & 0.2224 & 0.2189 & 0.2155 & 0.2130 & 0.2113 \end{bmatrix} \quad (5.7)$$

To find the values of the coefficients $A1 - A5$ that minimizes the function Q , the function *fminsearch* in MATLAB was used. The function *fminsearch* is an algorithm for unconstrained non-linear optimization.

The values of the unknown coefficients obtained by minimizing Equation 5.6 are shown in Equation 5.8. This resulted in a rather complex equation for calculating the reduced shear force capacity for a beam with a hole, $V_{k,hole}$ (Equation 5.9).

$$\begin{aligned} A1 &= 1.0125 \\ A2 &= -1.7008 \\ A3 &= 0.7837 \\ A4 &= 0.3823 \\ A5 &= -0.2976 \end{aligned} \quad (5.8)$$

$$\frac{V_{k,hole}}{h_w b_w f_t} = (1.0125 - 1.7008(\frac{d}{h_w}) + 0.7837(\frac{d}{h_w})^2 + 0.3823(\frac{h_f^2}{b_w l_1})(\frac{h_w}{EG_f/f_t^2})^{-0.2976} \quad (5.9)$$

Equation 5.9 includes the material parameters that were included also in the parameter study and is based on the beams with one circular hole. The equation is not verified and is at this stage not recommended for design calculations. As for the plots in the parameter study, this equation is only valid for the the current load situation, and can not be used in a general case. Figure 5.8 shows the results from the parameter study compared to the results from using Equation 5.9.

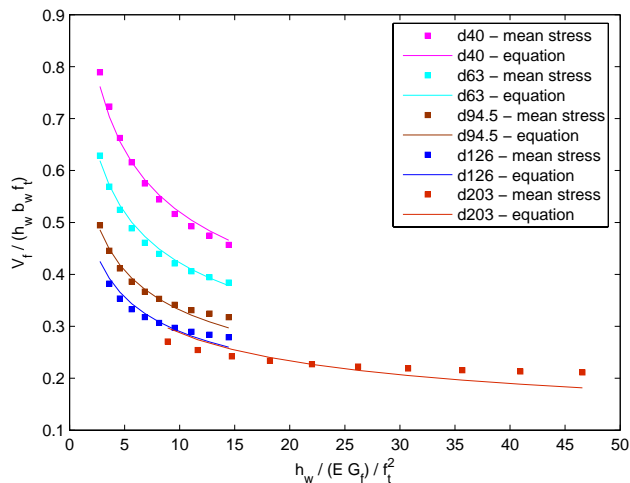


Figure 5.8: *The shear force capacity V_f from the parameter study and from using the new Equation 5.9.*

Chapter 6

Conclusions

6.1 Concluding remarks

The work with this master's thesis has resulted in conclusions that will be discussed in this section.

By studying the angles to the location of the maximum of the first principal stress at the edge of the hole and three and eight nodes outside the hole (approximately three and eight mm outside the hole respectively), it was found that this angle can vary significantly from 45 °. It was also found that the angles for the outer paths differ very little from the angle at the edge of the hole, and the conclusion that a crack will grow in an angle perpendicular to the edge of the hole could thus be drawn.

In the calculations of the shear force capacity for beams with holes in the web, three criteria based on fracture mechanics theory were used. By comparing the ratio V_{theory}/V_{test} for the three criteria, where V_{test} is the shear force capacity from a previous test study of the same beam geometries and load cases, it was found that the mean stress criterion and the initial crack criterion are suitable for calculating the shear force capacity of beams with holes. The point stress criterion however was not suitable since this method severely underestimated the shear force capacity of some beams.

By evaluating the current method for calculating the reduced shear force capacity for beams with holes in the web used by Swelite and Forestia, it was found that this method does not give values corresponding well with the shear force capacity for the tested beams. For three of the types of beams studied the characteristic shear force capacity calculated by the current method was larger than the characteristic shear force capacity from the tests. This method also underestimated the shear force capacity for some beams considerably. The calculation method used by Swelite and Forestia does accordingly not seem very accurate and suitable for calculating the shear force capacity for beams with holes. An attempt was made to develop an alternative shear strength equation. This equation shows how the size of a circular hole and how the different material property parameters are predicted to affect the shear strength. The alternative equation can, however, at the present stage of

knowledge not be recommended for use in design. Further work on verification and generalization is needed.

6.2 Future work

During the work with this thesis, some areas that need further investigation have sprung to mind, and these are mentioned in this section.

- The calculations in this study have been compared to previous tests including 11 beam geometries. The mean stress method needs to be verified further by comparison to more empirical results.
- The new calculation method suggested in this study was based on the results from primarily the beam height 220 mm. A further development of these calculation methods based on more beam heights is needed as well as verification of the equations.
- A more general calculation method, that is valid for various load cases is needed.

Bibliography

- [1] American Forest and Paper Association, (1999) *Allowable Stress Design - Manual For Engineered Wood Constructions*.
- [2] Burström, P-G. (2001) *Byggnadsmaterial - Uppbyggnad, tillverkning och egenskaper*. Studentlitteratur, Lund.
- [3] Danewid, R., Johansson, C-J. and Isaksson, T. (2000) *Träkonstruktioner*. Division of Structural Engineering, Lund University, Lund.
- [4] European Organisation for Technical Approvals. (2004) *European Technical Approval No. ETA-02/0026*, VTT rakennus- ja yhdyskunta tekniikka, Espoo.
- [5] European Organisation for Technical Approvals. (2004) *European Technical Approval No. ETA-03/0056*, Norwegian Building Research Institute, Oslo.
- [6] Gustafsson, P-J. (2002) *Mean stress approach and initial crack approach*. Report "Fracture Mechanics Models for Strength Analysis of Timber Beams with a Hole or a Notch" of RILEM TC-133, Lund University, Lund.
- [7] <http://www.gp.com>, (2005) Homepage of Georgia-Pacific.
- [8] <http://www.i-joist.org/home.asp>, (2005) Wood I-Joist Manufacturers Association.
- [9] <http://www.swelite.se>, (2005) Homepage of Swelite.
- [10] Landelius, J. (1989) *Finit Area Metoden - en bra metod för beräkning av uppfläkningsbrott?* Report TVSM-5043, Lund Institute of Technology, Lund.
- [11] Morris, V., Gustafsson, P-J. and Serrano, E. (1995) *The shear strength of light-weight beams with and without a hole - a preliminary study*. COST 508 - Wood Mechanics Proc. of the 1995 Wood Mechanics Workshop on Mechanical Properties of Panel Products. Watford, UK.
- [12] Nordtest Method. (1993) *WOOD: Fracture Energy in Tension Perpendicular to the Grain*, NT BUILD 422 Project 944-90, Gustafsson, P-J. and Larsen, H-J., Espoo, Finland.

- [13] Persson, K., Gustafsson, P.-J. and Petersson, H. (1993) *Influence of plastic dissipation on apparent fracture energy determined by a three-point bending test*. Proc. of COST 508 Workshop on "Wood: Plasticity and Damage", Editors: Birkinshaw, C., Morlier, P. and Seoane, I., University of Limerick, pp. 123-133.
- [14] Serrano, E. (2004) *Verification of a design formula for i-joists with web holes*. Reference P401434, Swedish National Testing and Research Institute, Borås.
- [15] Swelite. (2005) *Projekteringsanvisningar*, edition 2005:1, Rundvik.
- [16] The MathWorks, Inc. (2004) *MATLAB Help - Functions*.

Appendix A

Stress distribution in beams

This appendix includes figures showing the distribution of the maximum of the first principal stress in the beams from Chapter 3. The load cases are described by the notation (N, V, M) where N = the normal force, V = the shear force and M = the bending moment. The units of (N, V, M) are [N, N, Nmm] and the unit of the first principal stress in the colorbar is [MPa].

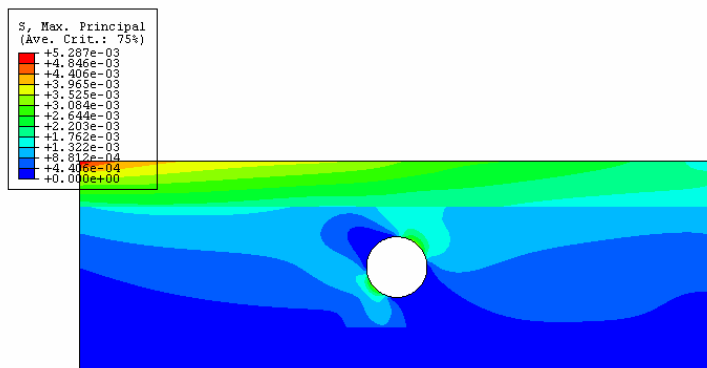
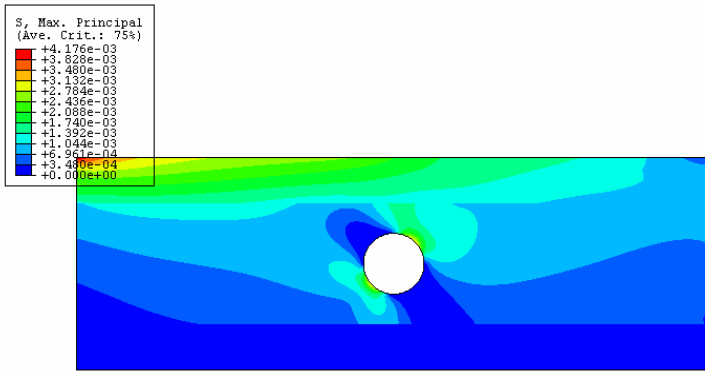
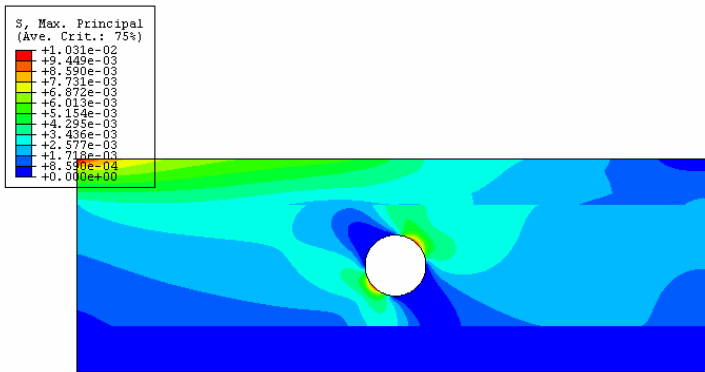
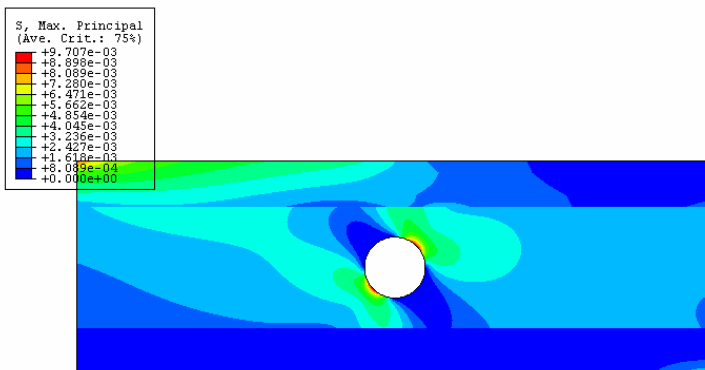


Figure A.1: Load case $(N, V, M) = (0, -1, -990)$.

Figure A.2: Load case $(N, V, M) = (0, -1, -660)$.Figure A.3: Load case $(N, V, M) = (0, -3, -1320)$.Figure A.4: Load case $(N, V, M) = (0, -3, -770)$.

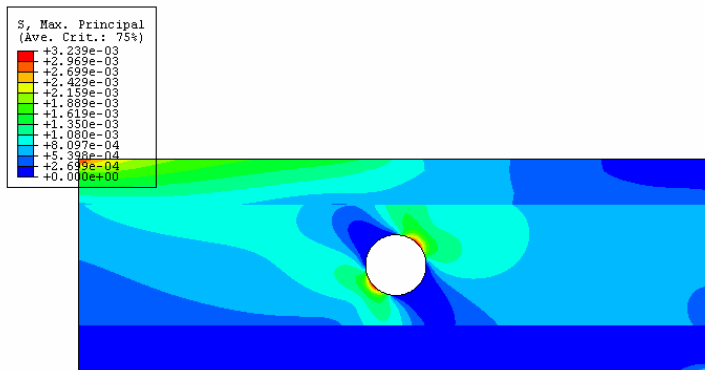


Figure A.5: Load case $(N, V, M) = (0, -3, -660)$.

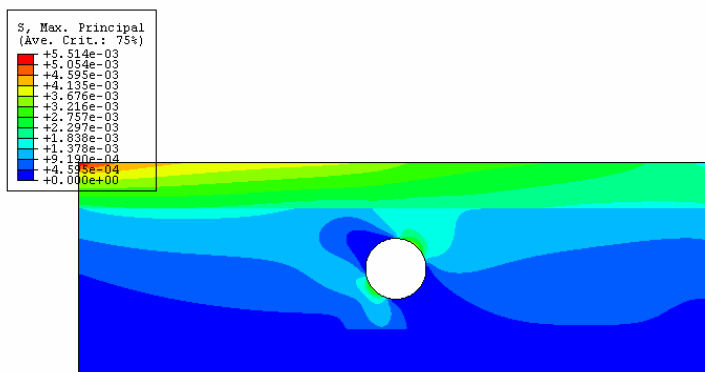


Figure A.6: Load case $(N, V, M) = (1, -1, -990)$.

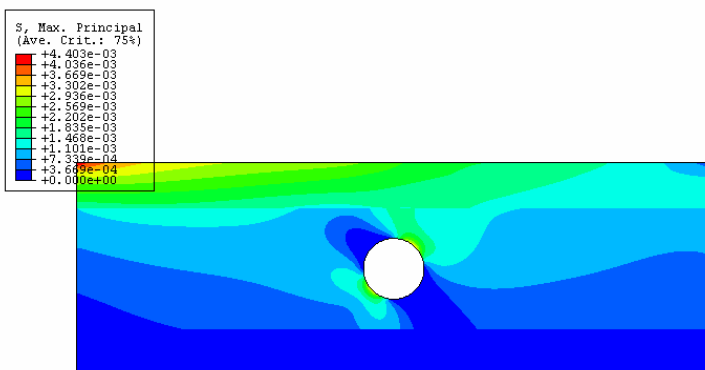
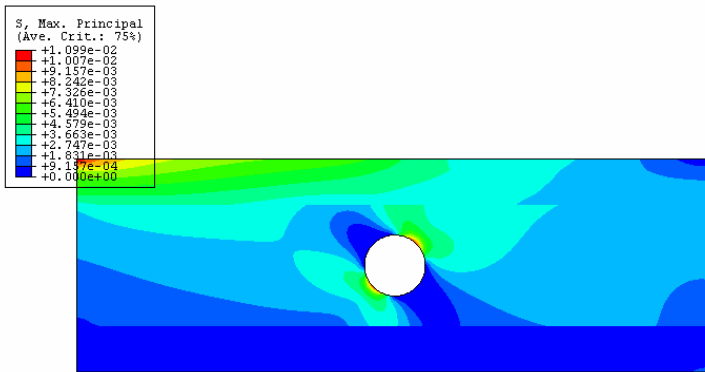
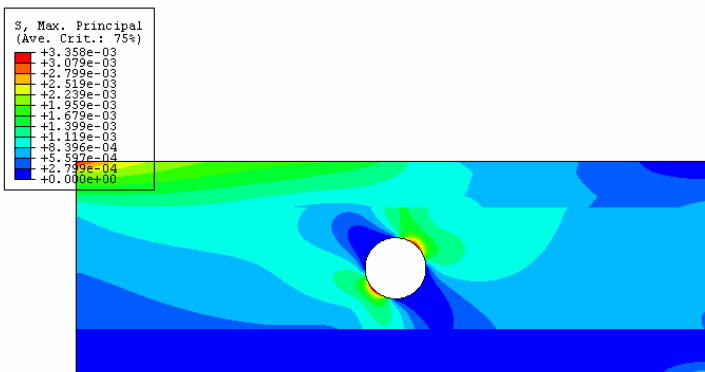
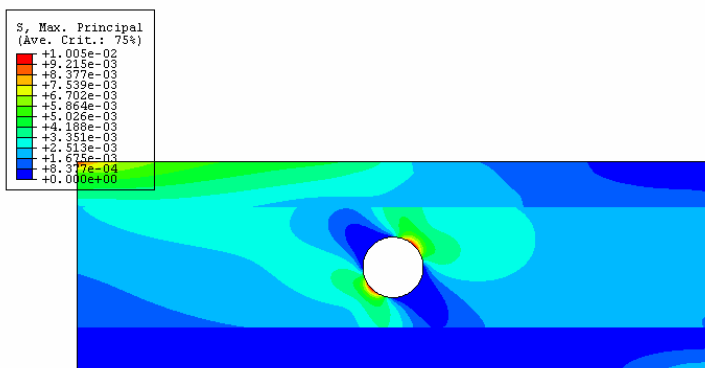


Figure A.7: Load case $(N, V, M) = (1, -1, -660)$.

Figure A.8: Load case $(N, V, M) = (3, -3, -1320)$.Figure A.9: Load case $(N, V, M) = (1, -1, -330)$.Figure A.10: Load case $(N, V, M) = (3, -3, -770)$.

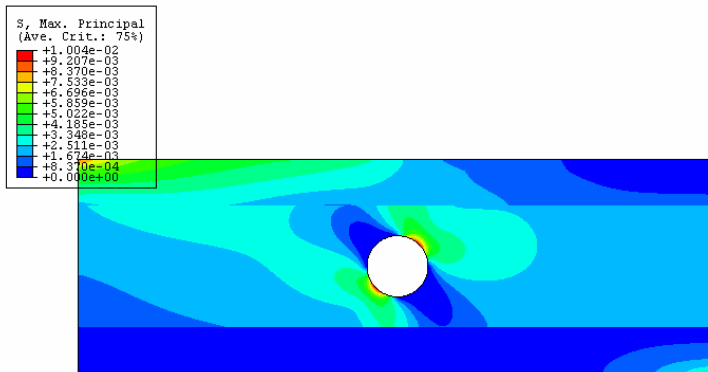


Figure A.11: Load case $(N, V, M) = (3, -3, -660)$.

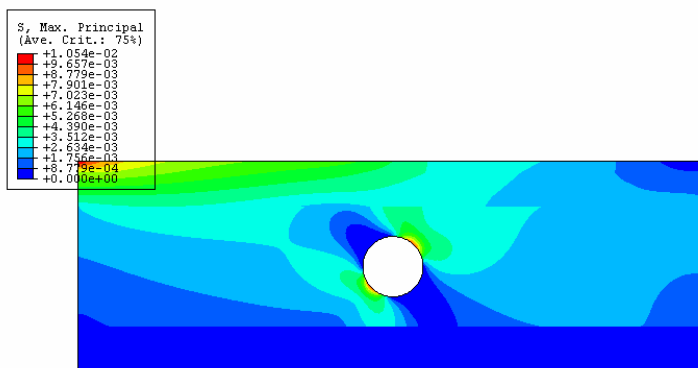


Figure A.12: Load case $(N, V, M) = (1, -3, -1320)$.

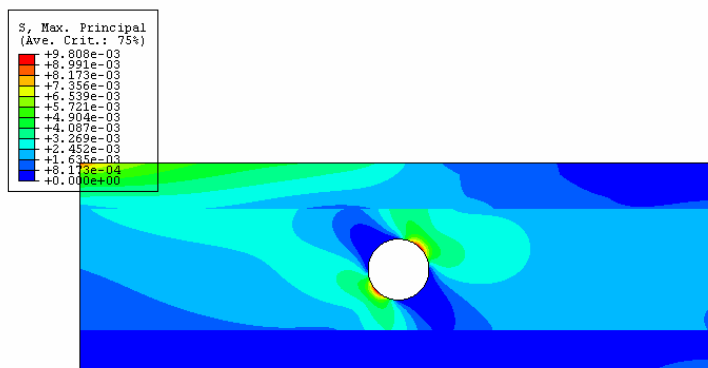
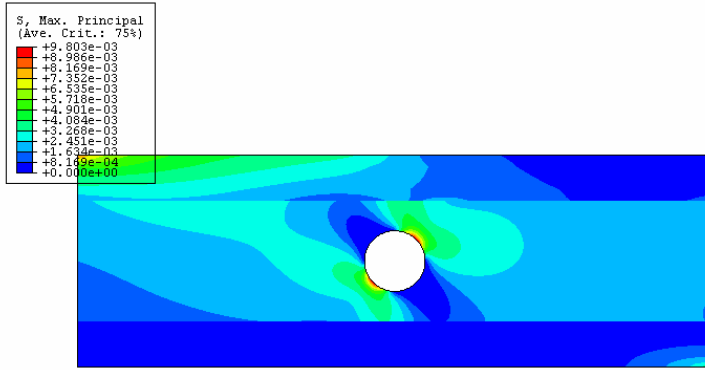
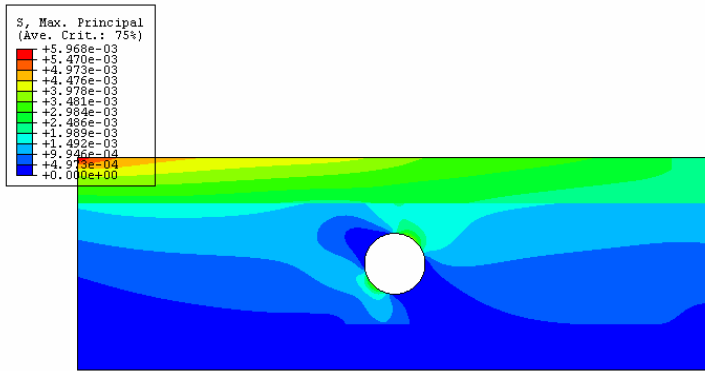
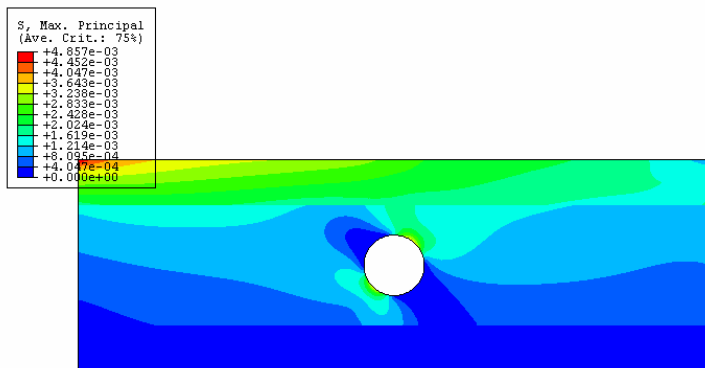


Figure A.13: Load case $(N, V, M) = (1, -3, -770)$.

Figure A.14: Load case $(N, V, M) = (1, -3, -660)$.Figure A.15: Load case $(N, V, M) = (3, -1, -990)$.Figure A.16: Load case $(N, V, M) = (3, -1, -660)$.

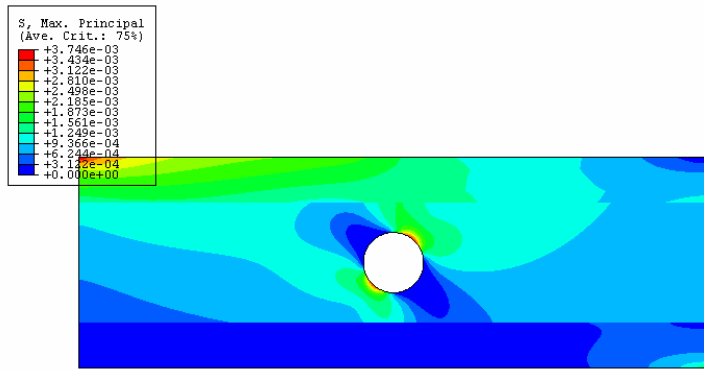


Figure A.17: Load case $(N, V, M) = (3, -1, -330)$.

Appendix B

Mean stress plots

This appendix includes plots showing the mean value of the first principal stress over the distance x from the edge of the hole, in the assumed crack direction.

